

# Deep-Sea Research Part I

## Deep Pacific Circulation: new insights on pathways through the Solomon Sea --Manuscript Draft--

<b>Manuscript Number:</b>	DSR1-D-20-00265R1
<b>Article Type:</b>	Research Paper
<b>Section/Category:</b>	Physical Oceanography
<b>Keywords:</b>	Deep water masses; Southwest Pacific; Throughflow variability; Diapycnal mixing
<b>Corresponding Author:</b>	Cyril Germineaud, Ph.D University of Miami Miami, Florida UNITED STATES
<b>First Author:</b>	Cyril Germineaud, Ph.D
<b>Order of Authors:</b>	Cyril Germineaud, Ph.D Sophie Cravatte, Ph.D Janet Sprintall, Ph.D Marion Sophia Alberty, Ph.D Mélanie Grenier, Ph.D Alexandre Ganachaud, Ph.D
<b>Abstract:</b>	<p>In the South Pacific Ocean, upper and lower Circumpolar Deep Water (UCDW and LCDW, respectively) occupy the deep layers; however, the presence and fate of both these water masses in the western equatorial Pacific have been mostly based on sparse measurements in both space and time. In this study, unprecedented deep measurements from three cruises conducted in the Solomon Sea region along with the World Ocean Atlas 2018 database are examined to better characterize the properties and pathways of deep water in the Southwest Pacific. At depths encompassing most of the UCDW, estimated transports derived from two inverse model solutions indicate interbasin exchanges between the Solomon Sea Basin and the Coral Sea Basin to the south and the East Caroline Basin to the north. The deep water transport variability found across the Solomon Sea is consistent with observed water mass modifications due, for the most part, to diapycnal mixing. At depths greater than about 2600 m, deep water inflow into the Solomon Sea Basin is limited to the south, emanating from the Coral Sea remote basins via complex trench topography. Spreading of LCDW in the Coral Sea and subsequently into the Solomon Sea is blocked by the Tonga-Kermadec Ridge to the east and bottom topography to the south, however, the densest part of UCDW entering both the Coral and Solomon Seas is likely influenced by LCDW properties, as oxygen is found to increase and silicate decrease with depth in the region. Waters trapped in closed deep basins, in the Bismarck Sea below 1750 m and the northern Solomon Sea below 3500 m show a remarkably constant pattern in oxygen with depth.</p>
<b>Suggested Reviewers:</b>	Stephen R Rintoul, Dr Oceanographer, CSIRO: Commonwealth Scientific and Industrial Research Organisation steve.rintoul@csiro.au  Gregory C Johnson, Dr Oceanographer, NOAA Pacific Marine Environmental Laboratory gregory.c.johnson@noaa.gov  Herle Mercier, Dr Oceanographer, LOPS: Laboratoire d'Océanographie Physique et Spatiale herle.mercier@ifremer.fr
<b>Opposed Reviewers:</b>	
<b>Response to Reviewers:</b>	

# 1 **Deep Pacific Circulation: new insights on pathways through the**

## 2 **Solomon Sea**

3 C. Germaineaud<sup>1,2,\*</sup>, S. Cravatte<sup>3</sup>, J. Sprintall<sup>4</sup>, M. S. Albery<sup>5</sup>, M. Grenier<sup>3</sup> and A. Ganachaud<sup>3</sup>

4 <sup>1</sup>Cooperative Institute for Marine and Atmospheric Studies, University of Miami, Miami,  
5 Florida, USA.

6 <sup>2</sup>NOAA/Atlantic Oceanographic and Meteorological Laboratory, Physical Oceanography  
7 Division, Miami, Florida, USA.

8 <sup>3</sup>Laboratoire d'Etudes en Géophysique et Océanographie Spatiales, Université de Toulouse,  
9 CNES, CNRS, IRD, UPS, Toulouse, France.

10 <sup>4</sup>Scripps Institution of Oceanography, University of California, San Diego, California, USA.

11 <sup>5</sup>Geophysical Fluid Dynamics Laboratory, Princeton University, Princeton, New Jersey, USA.

12 *Corresponding Author:*

13 Cyril Germaineaud

14 CIMAS, University of Miami and NOAA/AOML/Physical Oceanography Division,

15 4301 Rickenbacker Causeway, Miami, FL 33149, USA.

16 *E-mail:* [cyril.germaineaud@gmail.com](mailto:cyril.germaineaud@gmail.com)

### 17 **Highlights**

18 ● Solomon Sea deep waters are supplied from the Coral Sea and East Caroline Basins

19 ● Deep water transport variability is significant across the Solomon Sea

20 ● Deep water mass modifications are due to diapycnal exchanges in the Solomon Sea

21 *\*Present address:*

22 Laboratoire d'Etudes en Géophysique et Océanographie Spatiales, Université de Toulouse,

23 14 Avenue E. Belin, 31400 Toulouse, France.

24 **Abstract**

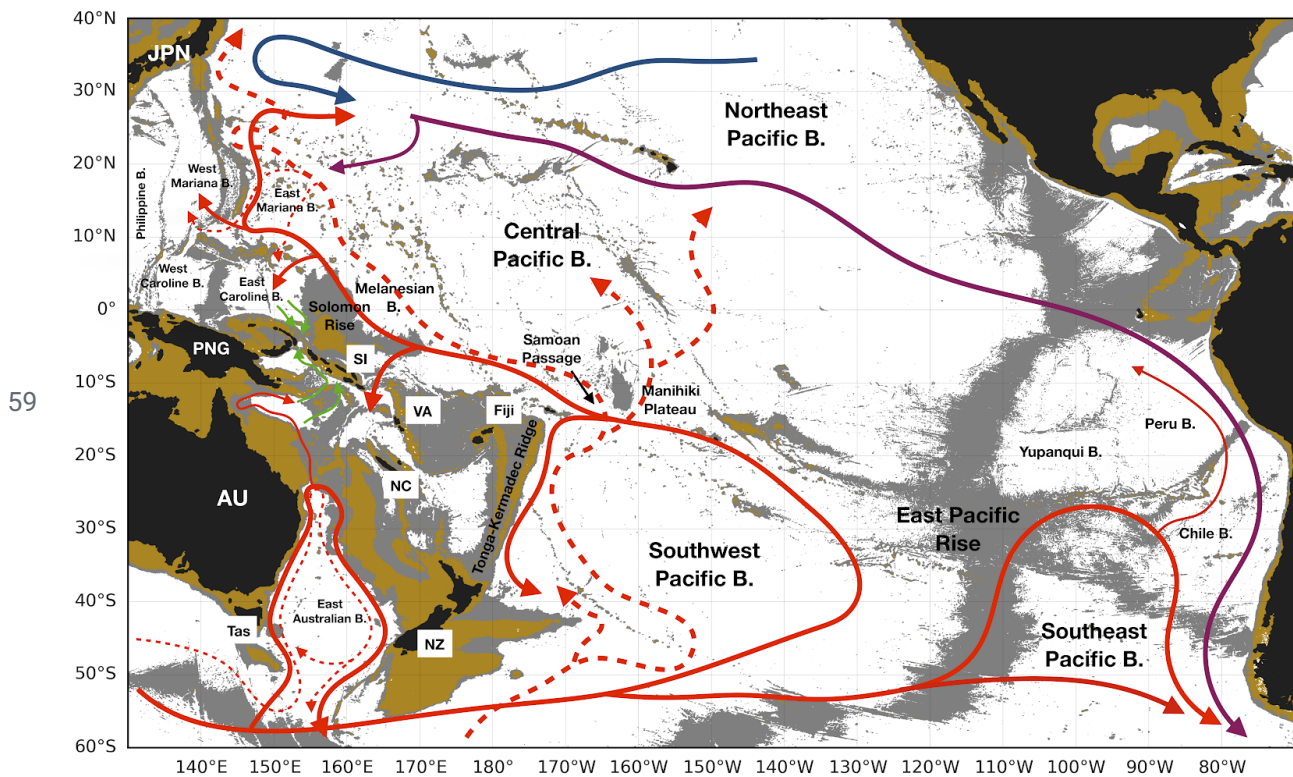
25 In the South Pacific Ocean, upper and lower Circumpolar Deep Water (UCDW and LCDW,  
26 respectively) occupy the deep layers; however, the presence and fate of both these water masses  
27 in the western equatorial Pacific have been mostly based on sparse measurements in both space  
28 and time. In this study, unprecedented deep measurements from three cruises conducted in the  
29 Solomon Sea region along with the World Ocean Atlas 2018 database are examined to better  
30 characterize the properties and pathways of deep water in the Southwest Pacific. At depths  
31 encompassing most of the UCDW, estimated transports derived from two inverse model  
32 solutions indicate interbasin exchanges between the Solomon Sea Basin and the Coral Sea Basin  
33 to the south and the East Caroline Basin to the north. The deep water transport variability found  
34 across the Solomon Sea is consistent with observed water mass modifications due, for the most  
35 part, to diapycnal mixing. At depths greater than about 2600 m, deep water inflow into the  
36 Solomon Sea Basin is limited to the south, emanating from the Coral Sea remote basins via  
37 complex trench topography. Spreading of LCDW in the Coral Sea and subsequently into the  
38 Solomon Sea is blocked by the Tonga-Kermadec Ridge to the east and bottom topography to the  
39 south, however, the densest part of UCDW entering both the Coral and Solomon Seas is likely  
40 influenced by LCDW properties, as oxygen is found to increase and silicate decrease with depth  
41 in the region. Waters trapped in closed deep basins, in the Bismarck Sea below 1750 m and the  
42 northern Solomon Sea below 3500 m show a remarkably constant pattern in oxygen with depth.

43 **Keywords**

44 Deep water masses; Southwest Pacific; Throughflow variability; Diapycnal mixing

45 **1 Introduction**

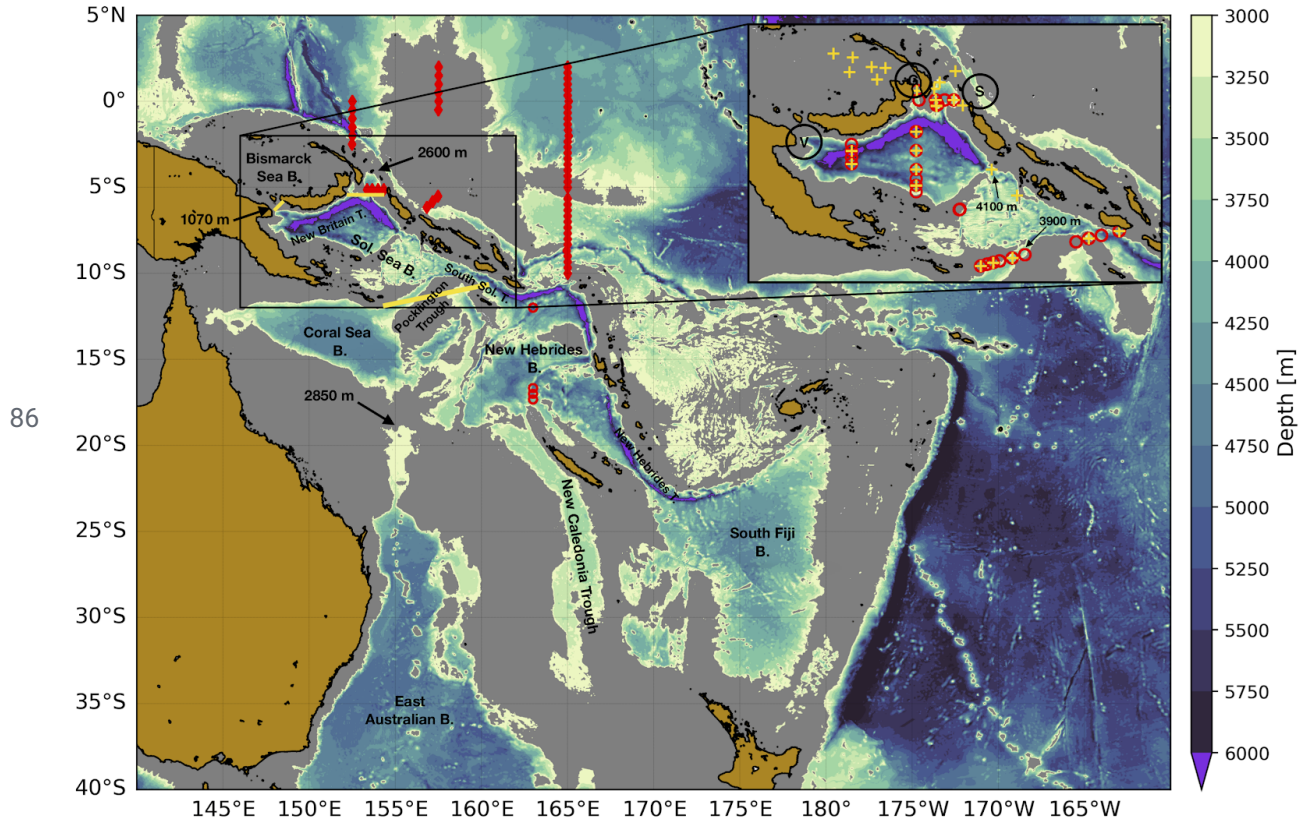
46 Over the past decade, several studies have highlighted the key contribution of the deep  
47 (2000-4000 m) and abyssal (depths > 4000 m) oceans in accumulating excess heat from the  
48 surface (e.g., Johnson et al., 2015; Purkey and Johnson, 2010), with large contributions from the  
49 Southern Ocean and the South Pacific Ocean (Desbruyères et al., 2016; Purkey et al., 2019;  
50 Meinen et al., 2020). However, to be able to properly assess and monitor this observed heat  
51 uptake from the oceans below 2000 m, it is important to have a better understanding of the water  
52 circulation and properties in the deep and abyssal layers. In the Pacific Ocean, the abyssal waters  
53 originate from the Southern Ocean, as a mixture between dense and cold water from the  
54 Antarctic Bottom Water (AABW) and the densest part of the overlying Circumpolar Deep  
55 Water (CDW) at the northern edges of the Antarctic Circumpolar Current (ACC; Mantyla and  
56 Reid, 1983; Orsi et al., 1999; Johnson, 2008). Most of this mixture enters the Pacific Ocean via  
57 the Southwest Pacific Basin, the only major basin that remains open to the Northern Hemisphere  
58 below 3500 m (see Fig. 1; Tsimplis et al., 1998).



59  
60 **Fig. 1:** Map of the Pacific Ocean south of 40°N. Brown shading shows bathymetry above 2000 m; gray shading  
61 indicates areas at depths of 2000 to 3500 m from the gridded 30 arc-second General Bathymetric Chart of the  
62 Oceans (GEBCO) 2020. Solid red lines with arrows indicate schematic pathways of the Upper Circumpolar Deep  
63 Water (UCDW); solid blue line shows the flow of North Pacific Deep Water (NPDW) and solid purple lines indicate  
64 modified NPDW flow. These pathways are based on the study of Siedler et al. (2004) and Figure 2b of Kawabe and  
65 Fujio (2010). Paths of the Lower Circumpolar Deep Water (LCDW) are in dashed red lines based on Figure 2c of  
66 Kawabe and Fujio (2010), Figure 15 of Siedler et al. (2004) and Figure 16f of Sokolov and Rintoul (2000) in the

67 East Australian Basin, in which the thin solid red line represents the Antarctic Circumpolar Current bottom water  
68 (ACCbw). Schematic pathways of UCDW above sill depths into the Solomon Sea Basin (green lines with arrows)  
69 based on this study are also indicated. Country/Island names are indicated as follows: Australia (AU); Japan (JPN);  
70 New Caledonia (NC); New Zealand (NZ); Papua-New Guinea (PNG); Solomon Islands (SI); Tasmania (Tas) and  
71 Vanuatu (VA). Note that B. = Basin.

72 On the western boundary of the Southwest Pacific Basin, the Tonga-Kermadec Ridge prevents  
73 abyssal water inflow into the intricate and remote deep basins east of Australia, and subsequently  
74 into the Solomon Sea Basin, which is connected at great depths to the New Hebrides Basin via  
75 the South Solomon Trench (see Fig. 2 for locations). South of 12°S, the New Hebrides Basin is  
76 connected to the South Fiji Basin via the South New Hebrides Trench. At depths greater than  
77 3000-3250 m, these basins are also isolated from the Central Pacific Basin, as possible inflow is  
78 blocked by shallow topography east of the Solomon Islands. North of 8°S, the Solomon Sea is  
79 strongly constrained by three narrow passages. The westernmost passage named Vitiaz Strait  
80 (147.6°E, 6°S) is closed to the north below a sill depth of 1070 m. To the east, St George's  
81 Channel (153.4°E, 4°S) has a sill depth of about 1400 m. The Solomon Strait (153.4°E, 4°S) is  
82 much deeper, but topography prevents flow paths deeper than 2600 m. The Solomon Sea was  
83 assumed to be isolated from the deeper thermohaline circulation pathways, and the ventilation of  
84 deep waters in this area, which at some locations reach depths greater than 9000 m, remains  
85 undocumented.



87 **Fig. 2:** Bathymetry below 3000 m of the western Pacific Ocean (140°E-160°W, 40°S-10°N) from the  
 88 gridded 30 arc-second General Bathymetric Chart of the Oceans (GEBCO) 2020; the inset provides a  
 89 closer view of the Solomon Sea. Grey shading indicates locations where bathymetry (or bottom depth) is  
 90 shallower than 3000 m, and critical sill depths (black arrows) are indicated. Hydrographic stations with  
 91 measurements deeper than 2000 m depth are shown for the Pandora cruise (July 2012; red circles),  
 92 MoorSPICE cruise (March 2014; yellow crosses) and Cassiopée cruise (July-August 2015; red  
 93 diamonds). The transects defining the boundaries of the inverse model are indicated as yellow lines; the  
 94 circled V, S and G (see inset) represent Viti Strait, Solomon Strait, and St George's Channel,  
 95 respectively. Sol. = Solomon; B. = Basin and T. = Trench.

96 Hydrographic data in the subtropical Pacific have been previously limited to four main sections  
 97 (<http://whp-atlas.ucsd.edu/pacific/sections.htm>) collected in the 1990s as part of the World Ocean  
 98 Circulation Experiment (WOCE): the P06 (153.3°E-71.5°W, 30°S-32°S), P11S (155°E,  
 99 11.4°S-43.2°S), P14C (175.2°E-177.6°E, 18.3°S-35.4°S) and P21 (153.4°E-75.1°W,  
 100 15.3°S-24.6°S). More recently, these sections were reoccupied under the international Global  
 101 Ocean Ship-based Hydrographic Investigations Program (GO-SHIP), but a large part of the deep  
 102 and abyssal waters in the western equatorial Pacific (145°E-165°W, 15°S-15°N) remains poorly  
 103 sampled, or even completely unexplored. Indeed, a comprehensive set of *in situ* hydrographic  
 104 measurements in the Solomon Sea region was, until recent years, mostly based on a few

105 full-depth observations collected during the Western Equatorial Pacific Ocean Circulation  
106 Studies (WEPOCS) expeditions in the mid-1980s (e.g., Lindstrom et al., 1987).

107 As part of the Southwest Pacific Ocean Circulation and Climate Experiment (SPICE), two  
108 cruises extensively explored the Solomon Sea region in July 2012 and March 2014 (Ganachaud  
109 et al., 2017). Full-depth and high-resolution hydrographic transects were performed in the  
110 Solomon Sea and the surroundings during both cruises (see Fig. 2). A striking feature found  
111 during both cruises was the high oxygen signature in several occupied stations at depths greater  
112 than 3000 m in the Solomon Sea suggesting ventilation and the presence of the densest portion of  
113 the CDW. This new finding raises two main questions: (1) considering the topographic  
114 blockages, where does this deep water inflow come from? and (2) what are the water properties  
115 and the corresponding volume transport of this deep flow at the western boundary of the  
116 Southwest Pacific Basin?

117 Our study aims to investigate these two questions and give insights as to the broader implications  
118 of the deep and abyssal South Pacific Oceans. In the following, Section 2 will provide a  
119 background on our current understanding of the main deep water mass properties and their  
120 associated flow paths. In Section 3, we present the different datasets and methods of analysis.  
121 Section 4 describes the deep water mass properties in the western equatorial Pacific and provides  
122 transport estimates from inverse model solutions for each SPICE cruise. In Section 5, a  
123 comprehensive view of the deep water mass property distributions across the intricate Southwest  
124 Pacific region is discussed, before ending with some concluding remarks in Section 6.

## 125 **2 Background: Deep Pacific Ocean circulation**

126 At about 50°S from 150°E to 90°W, the Southern Ocean deep and bottom waters separate from  
127 the ACC and enter the South Pacific Ocean via the East Australian Basin, the Southwest Pacific  
128 Basin and the Southeast Pacific Basin (Fig. 1). In the Southern Ocean, Orsi et al. (2002) selected  
129 distinct neutral density surfaces ( $\gamma^n$ ) to divide the deep ocean: 28.27  $\gamma^n$  (~ 3000 m) to separate  
130 AABW from the lower part of the CDW (LCDW), 27.98  $\gamma^n$  (~ 2000 m) marking the limit with  
131 the upper part of the CDW (UCDW), and 27.7  $\gamma^n$  (~ 1000 m) defining the top of the UCDW.  
132 Note that in the ACC region, the densest layer of the LCDW ( $28.18 < \gamma^n < 28.27$ ) is referred to as  
133 the ACC bottom water (ACCbw; Orsi et al., 1999). The ACCbw and the two portions of the  
134 CDW are exported into the South Pacific basins, however, the AABW is confined by the ridge  
135 systems south of 50°S (Orsi et al., 1999). In the following, our current knowledge of the  
136 pathways and relevant water mass properties associated with the ACCbw and the two portions of  
137 the CDW across the Pacific Ocean are presented. The distinct property values identified in past  
138 studies to trace these deep water masses vary with latitude across the western Pacific Ocean; they  
139 are summarized for the region 145°E-165°W, 25°S-15°N in Table 1.

Water mass	Depth (m)	$\Theta$ (°C)	S (PSS-78)	O <sub>2</sub> ( $\mu\text{mol.kg}^{-1}$ )	SiO <sub>4</sub> ( $\mu\text{mol.kg}^{-1}$ )
UCDW	2000-3500	1.2-2.2	34.64-34.7	130-150	100-140
NPDW <sub>m</sub>	2000-3500	1.2-2	34.58-34.68	110-130	140-155
LCDW	3500+ m	< 1.2	34.685-34.73	> 155	110-142

140 **Table 1:** Characteristics of known deep water types in the Pacific Ocean north of 25°S to 15°N.  
141 Boundaries of UCDW properties are derived from Kawabe et al. (2009) and Sokolov and Rintoul (2000);  
142 The NPDW<sub>m</sub> and LCDW properties are based on corresponding property values identified by Siedler et  
143 al. (2004) and Wijffels et al. (1998).

### 144 **2.1 Antarctic Circumpolar Current bottom water and Lower Circumpolar Deep Water**

145 In the East Australian Basin, both the ACCbw and LCDW are blocked by topography north of  
146 20°S (Sokolov and Rintoul, 2000), and so turn southward and ultimately recirculate  
147 northwestward along the coast of Tasmania (Tsimplis et al., 1998) or feedback to the ACC  
148 system (red dashed lines in Fig. 1). East of the East Pacific Rise, the ACCbw is confined to the  
149 Southeast Pacific Basin, while the lightest LCDW is able to proceed northeastward into the Chile  
150 Basin, and then into the Peru Basin over sills shallower than 4000 m (Tsimplis et al., 1998). Most  
151 of the ACCbw and LCDW are transported in the Southwest Pacific Basin as a Deep Western  
152 Boundary Current (DWBC) along the Tonga-Kermadec Ridge (Whitworth III et al., 1999).  
153 Around 10°S, LCDW enters the Central Pacific Basin through the Samoan Passage and along the  
154 eastern side of the Manihiki Plateau (Roemmich et al., 1996; Rudnick, 1997; Voet et al., 2014,  
155 2016), while ACCbw is blocked south of the Samoan Passage (Orsi et al., 1999) and returns  
156 southward (Reid, 1997).

157 At depths greater than 3500 m, LCDW is found below potential temperatures of  $\theta = 1.2^\circ\text{C}$   
158 (Siedler et al., 2004; Kawabe and Fujio, 2010), and is characterized by a salinity (S) maximum  
159 and a silicate (SiO<sub>4</sub>) minimum (Orsi et al., 1999; Warren, 1973). Along the zonal WOCE P06  
160 section in the Southwest Pacific, Whitworth III et al. (1999) found high dissolved oxygen (O<sub>2</sub>)  
161 concentrations (180-214  $\mu\text{mol.kg}^{-1}$ ) associated with LCDW, while north, in the East Mariana  
162 Basin, the O<sub>2</sub> concentration below 3500 m only reaches values between 155 to 180  $\mu\text{mol.kg}^{-1}$   
163 (Siedler et al., 2004; Wijffels et al., 1998). As LCDW proceeds northward within the Central  
164 Pacific Basin, it splits into two branches, which eventually reach the Northeast Pacific Basin via  
165 complicated and narrow passages (e.g., Siedler et al., 2004; Kawabe et al., 2006). On its northern  
166 route, the LCDW accumulates silicate from bottom sediments (Alford et al., 2013; Talley and  
167 Joyce, 1992; Toole et al., 1994; Roemmich et al., 1996), associated with a decrease in O<sub>2</sub> before



168 being upwelled in the upper deep layers and ultimately transformed into North Pacific Deep  
169 Water (NPDW) via diapycnal mixing north of 40°N (e.g., Johnson et al., 2006).

170 These previous studies provide good overall pictures of the ACCbw and LCDW pathways and  
171 associated water properties in the Pacific Ocean; however, it is apparent that more detailed and  
172 accurate views of the circulation at near-bottom levels warrant further investigation. In this study,  
173 our results will confirm that LCDW does not spread to the Southwest Pacific basins, but it can  
174 imprint the overlying UCDW with its high oxygen signature.

## 175 **2.2 Upper Circumpolar Deep Water and North Pacific Deep Water**

176 According to previous studies, UCDW is characterized by an O<sub>2</sub> minimum (Callahan, 1972;  
177 Talley et al., 2007) and nutrient maxima (Warren, 1973; Whitworth III et al., 1999). At about  
178 20°S in the East Australian Basin, UCDW enters the Coral Sea with a transport of 3 Sv (Sokolov  
179 and Rintoul, 2000) based on the observations of the WOCE P11 section. Sokolov and Rintoul  
180 (2000) suggested that UCDW found in the eastern part of the Coral Sea is primarily supplied by  
181 waters coming from the Central Pacific Basin, and that UCDW entering from the east may flow  
182 into the South Solomon Trench, before continuing northward across the Solomon Sea (Sokolov  
183 and Rintoul, 2000; see their Figure 16f).

184 Nevertheless, the path of this deep inflow is rather uncertain as it is based on relatively scarce  
185 measurements. The  $\theta$ -S curves described by Sokolov and Rintoul (2000; their Figure 12) within  
186 the Solomon Sea, at Vitiaz Strait, St George's Channel, Solomon Strait and in the New Britain  
187 Trench were similar to those shown for the South Solomon Trench. This indicated homogeneous  
188 distributions of water mass properties throughout the Solomon Sea, which were cooler and  
189 fresher than those entering the Coral Sea further to the South from the East Australian Basin.  
190 Additionally, clear differences in both  $\theta$  and S between the East Caroline Basin and the northern  
191 part of the Solomon Sea suggested a limited deep inflow of northern origin through the Solomon  
192 Strait. As shown below, the results of the two SPICE cruises and Cassiopée rather suggest that  
193 exchanges of UCDW between the Solomon Sea Basin and the East Caroline Basin can occur,  
194 and that the primary source of UCDW in the Solomon Sea is the Coral Sea Basin, as initially  
195 suggested by Wyrski (1961).

196 At about 50°S east of 120°W, UCDW can enter the Southeast Pacific Basin before continuing  
197 northeastward into the Chile Basin (Fig. 1). Although the UCDW waters might proceed further  
198 north into the Peru and Yupanqui Basins, since there is no blocking bathymetry, previous studies  
199 (e.g., Reid, 1986, 1997; Tsimplis et al., 1998) indicated that most of the UCDW turns southward  
200 near the coasts of South America before returning to the ACC. From 40°S to 10°S, west of  
201 120°W, an anticyclonic flow, which corresponds to the lower limb of the subtropical gyre,  
202 occupies the Southwest Pacific Basin at depths of about 2000 to 3500 m (Reid, 1997; Kawabe

203 and Fujio, 2010). As the UCDW flows into the Southwest Pacific Basin (red solid lines in Fig.  
204 1), waters are passing around the subtropical gyre before crossing the Samoan Passage (e.g.,  
205 Roemmich et al., 1996; Rudnick, 1997; Taft et al., 1991), though part of the UCDW flows  
206 southward along the Tonga-Kermadec Ridge and recirculates in the subtropical gyre (Reid,  
207 1997). Around 10°S, UCDW bifurcates northwestward and flows around the Solomon Rise (Fig.  
208 1), before reaching the East Caroline Basin and the East Mariana Basin found north of the  
209 Solomon Sea (Kawabe et al., 2006, 2009). UCDW proceeds northward in the North Pacific and  
210 enters the Philippine Sea. Then, UCDW spans eastward towards the Hawaiian Ridge, where it  
211 meets NPDW that flows eastward from the north near 30°N (Kawabe et al., 2009; Kawabe and  
212 Fujio, 2010).

213 As mentioned in the previous section, the NPDW is formed through mixing as LCDW upwells in  
214 the North Pacific, with the imprint of a strong SiO<sub>4</sub> content (> 170 μmol.kg<sup>-1</sup>) from the seabed  
215 (Talley and Joyce, 1992; Talley et al., 2007). Most of the NPDW can be traced through its  
216 SiO<sub>4</sub>-rich signature as it flows westward into the Northwest Pacific Basin, and then southward at  
217 about 170°W (Johnson et al., 2006; Kawabe and Fujio, 2010). UCDW and NPDW signatures  
218 converge around 25°N-170°E to ultimately form a modified NPDW (hereinafter NPDW<sub>m</sub>) that  
219 proceeds southeastward (eastward purple line in Fig. 1) in the eastern Pacific before  
220 encountering the South American coastline, and flows southward into the ACC in the Drake  
221 Passage (Kawabe et al., 2009; Talley et al., 2007). Previous studies (Johnson and Toole, 1993;  
222 Siedler et al., 2004) have also found high-SiO<sub>4</sub> concentrations in the Northwest Pacific around  
223 15°N, suggesting possible transport of NPDW<sub>m</sub> from the east to the southeastern boundary of the  
224 East Mariana Basin, and potentially also entering the East Caroline Basin (westward purple line  
225 in Fig. 1).

## 226 **3 Data and Inverse Model**

### 227 **3.1 Ocean historical, bathymetry and cruise data**

228 This study takes advantage of both historical measurements of  $\theta$  (calculated using the *in situ*  
229 temperature and absolute salinity fields, and a reference pressure at 0 dbar), S, O<sub>2</sub> and nutrients  
230 from the World Ocean Atlas 2018 (WOA18;  
231 <https://www.nodc.noaa.gov/OC5/woa18/pubwoa18.html>) collected from January 1, 1950 to  
232 December 31, 2018. Only profiles below 2000 m depth from the Ocean Station Data (OSD) and  
233 high-resolution Conductivity-Temperature-Depth (CTD) datasets in the western Pacific Ocean  
234 (120°E-160°W, 50°S-10°N) were considered here. Of these profiles, only those with quality flags  
235 indicating good data were considered.

236 To determine potential deep pathways in the Southwest Pacific region, areas associated with  
237 critical sill depths and relevant topographic blockages are identified using the General

238 Bathymetric Chart of the Oceans (GEBCO) gridded dataset (GEBCO Compilation Group, 2020),  
239 as well as *in situ* echo-sounding surveys available from the two SPICE cruises.

240 Under the SPICE program, the first cruise (known as Pandora on the *R/V L'Atalante*) was  
241 conducted from 27 June to 6 August 2012 along a meridional transect north of Nouméa (163°E,  
242 from 18°S to 9°S) and across the Solomon Sea (Fig. S1), while the second cruise (known as  
243 MoorSPICE on the *R/V Thomas G. Thompson*) explored both the Solomon Sea and the Bismarck  
244 Sea from 28 February to 31 March 2014 (Fig. S1). Overall, 83 and 57 stations were surveyed  
245 during Pandora and MoorSPICE, respectively. A thorough description of the collected data and  
246 associated processing is available in Ganachaud et al. (2017); we only present here relevant  
247 information for this study. It is also worth mentioning that nine subsurface moorings were  
248 deployed from July 2012 until March 2014 at Vitiaz Strait, St George's Channel and Solomon  
249 Strait to determine the distinct cross-passage flow variability (Alberty et al., 2019). However, the  
250 moored hydrographic and current measurements recorded at the deepest channel of Solomon  
251 Strait are limited to a maximum depth of 1700 m and so are not employed here. A third cruise  
252 (known as Cassiopée on the *R/V L'Atalante*) was conducted from 19 July to 23 August 2015  
253 (Delpech et al., 2020); during which 74 hydrographic stations were occupied north and east of  
254 the islands bounding the Solomon Sea, with three meridional transects performed at  
255 approximately 153.5°E, 157.7°E and at 165°E (Fig. S1).

256 During these three cruises, T, S and O<sub>2</sub> measurements were carried out using CTD and O<sub>2</sub>  
257 sensors, and a pair of Lowered-Acoustic Doppler Current Profilers (L-ADCPs) to measure  
258 currents. The pair of L-ADCPs was processed following Visbeck (2002). Absolute velocities  
259 were estimated using a least squares framework, including constraints on bottom velocity  
260 estimates from bottom-track pulses, navigational data and upper ocean velocities from the  
261 along-track shipboard ADCP data.

262 Discrete water samples were also obtained during the cruises with Niskin bottles to calibrate the  
263 CTD-O<sub>2</sub> sensors (S and O<sub>2</sub>) and for nutrient (nitrate NO<sub>3</sub>, phosphate PO<sub>4</sub> and SiO<sub>4</sub>)  
264 determination. A specific calibration was carried out for the O<sub>2</sub> sensor data by comparison with a  
265 Winkler titration determination of the water samples (Langdon, 2010; Uchida et al., 2010;  
266 Saout-Grit et al., 2015). During Pandora, 39 of the 164 casts were taken to depths greater than  
267 2000 m (red circles in Fig. 2), including repeat time series casts at 10 stations. During  
268 MoorSPICE, 30 of the 82 casts were carried out deeper than 2000 m (yellow crosses in Fig. 2)  
269 with repeat casts at 16 stations, while during Cassiopée, 56 of the 98 casts were deeper than 2000  
270 m (red diamonds in Fig. 2), and 26 stations were occupied multiple times.

271 The collected measurements during the three cruises were quality controlled following the  
272 GO-SHIP guidelines (Hood et al., 2010). We use in this study the cruise measurements identified

273 as “good data” for the CTD-O<sub>2</sub> profiles, and as “probably good data” (“good data” flag is not  
274 available) for the bottle water samples. It should also be noted that we only use here the SiO<sub>4</sub>  
275 samples collected during Pandora, because some measurement issues were found with the SiO<sub>4</sub>  
276 samples from the MoorSPICE and Cassiopée cruises at depths greater than 2000 m. Data from  
277 all three cruises are used to describe the water property characteristics of the deep waters but  
278 only the Pandora and MoorSPICE cruises are used in the inverse model. This is because, unlike  
279 the two SPICE cruises, the hydrographic transects performed during the Cassiopée cruise do not  
280 enclose the Solomon Sea across the entrances and exits.

## 281 **3.2 Inverse Model**

### 282 **3.2.1 Inversion Principle**

283 Linear inverse methods applied to hydrographic measurements (e.g., Ganachaud and Wunsch,  
284 2000; Lumpkin and Speer, 2007; Germaineaud et al., 2016) have been extensively used to  
285 estimate ocean circulation and associated transports within a finite ocean volume divided in  
286 different layers from the surface down to the bottom, and usually chosen to encompass major  
287 water masses. The classical procedure uses pairs of *in situ* temperature and salinity profiles along  
288 hydrographic transects to calculate an initial guess of geostrophic flow relative to a given  
289 reference level along with *a priori* velocity uncertainties, which can be, in practice, estimated  
290 from deep current meters or L-ADCP profiles. One can then use an inverse method to estimate  
291 an adjusted velocity field and corresponding transports with uncertainties to depict a more  
292 synoptic representation of the ocean circulation than the one inferred from the initial observed  
293 velocities. For this purpose, adjustments to the initial guess (*a priori* velocities) are typically  
294 made such that the revised circulation scheme satisfies basic conservation requirements of the  
295 total mass transport and water property fluxes (e.g., salt, heat and/or nutrients).

### 296 **3.2.2 Our Inverse Model**

297 Within the Solomon Sea, an inverse model based on Gauss-Markov estimation (Wunsch, 1996),  
298 is used to estimate synoptic transports of the deep flow during Pandora and MoorSPICE across  
299 three hydrographic transects enclosing the Solomon Sea (yellow lines in Fig. 2). Mass and  
300 property constraints are applied over 25 and 24 (during Pandora and MoorSPICE, respectively)  
301 isopycnal layers defined by potential density anomaly surfaces to derive adjusted velocities and  
302 transports with error estimates. The *a priori* velocities and the different model’s constraints are  
303 presented in the two following sections. As we focus on the deep circulation here, we will only  
304 present the nonadjusted (before inversion) and adjusted (after inversion) transports across the  
305 Solomon Sea for the deep layers, at depths greater than 1500 m. Note that even though Vitiaz  
306 Strait is closed below 1000 m depth, our inverse model conserves mass top-to-bottom within the  
307 Solomon Sea box. The *a priori* transport estimates across Vitiaz Strait in the upper 1000 m are  
308 thus also taken into account to derive the two inverse model solutions.

### 309 **3.2.3 Initial guess for the inverse calculation**

310 For both the Pandora and MoorSPICE cruises, shipboard ADCP (S-ADCP) profiles are used as *a*  
311 *priori* velocities rather than geostrophic velocities to take into account current pathways as close  
312 as possible to the coast over the upper 1000 m in the Solomon Sea. In addition, the outflow  
313 through Vitiaz Strait, St George's Channel and Solomon Strait is constrained by processes other  
314 than geostrophy. At the southern entrance (south of 10°S), at depths where the S-ADCP is not  
315 available (i.e., below 1000 m), we use geostrophic velocities calculated between CTD station  
316 pairs, and then interpolated on the S-ADCP grid using a Gaussian weighting function. A vertical  
317 smoothing was performed using a 10-m moving average filter to avoid large discontinuities at  
318 the transition between S-ADCP and geostrophy.

319 The S-ADCP currents were rotated to be perpendicular to the transect (following Germaineaud et  
320 al., 2016), then combined with the geostrophic velocity field. For the geostrophic part, an initial  
321 zero reference level was set at 3000 dbar, or, for shallower stations, at the deepest common level  
322 of station pairs along the transect at the southern entrance. L-ADCP profiles taken on CTD  
323 stations that were occupied more than once permitted the determination of initial reference  
324 velocities and associated uncertainties. Most of the cruise velocity profiles suggested velocities  
325 weaker than 5 cm s<sup>-1</sup> at depths ranging from 2000 to about 3000 m, and so initial reference  
326 velocities were chosen to be 0 ± 5 cm s<sup>-1</sup>. The outflow through Vitiaz Strait is limited to the  
327 upper 1000 m so only S-ADCP profiles are used as *a priori* velocities. To avoid estimates of  
328 unrealistic geostrophic flow across the northern transect between St George's Channel and  
329 Solomon Strait, a merged velocity field is built, based on S-ADCP velocities in the surface layer  
330 and L-ADCP profiles taken on CTD stations beneath the depth limit of the S-ADCP. Both  
331 S-ADCP and L-ADCP velocity profiles were first compared at overlapping depths, and only  
332 negligible discrepancies (< 1 cm s<sup>-1</sup>) were observed. L-ADCP velocities were then interpolated  
333 onto the S-ADCP grid using the same Gaussian weighting function as used for the southern  
334 transect. This merged ADCP velocity field is used as our initial guess for the transect between St  
335 George's Channel and Solomon Strait. A range of velocity adjustments was set to 0 ± 5 cm s<sup>-1</sup>  
336 based again on the repeated L-ADCP profiles recorded on stations along the section. Note that a  
337 similar ADCP velocity field was also built for the southern transect; however, large uncertainties  
338 in bottom track velocity estimates from the two paired L-ADCPs (especially during MoorSPICE)  
339 led to spurious strong velocities (> 15 cm s<sup>-1</sup>) at the deepest measurements.

340 We estimate the upper deep layer transport with uncertainties across the transect at the southern  
341 entrance and at the northeastern exit (through both St George's Channel and Solomon Strait), in  
342 one primary isopycnal layer bounded by 27.65 and 27.76  $\sigma_0$  (Table 2). The isopycnal  $\sigma_0 = 27.65$   
343 (~ 2000 m) is above  $\theta = 2.2^\circ\text{C}$ , which marks the transition of the lighter deep layer mixed with  
344 intermediate waters. Below,  $\sigma_0 = 27.76$  (~ 3250 m) approximately corresponds to the transition

345 from low to increasing S and O<sub>2</sub>. Both initial (before inversion) and adjusted (after inversion)  
346 transports are reported (see Table 2).

### 347 **3.2.4 Constraints on the adjusted flow**

348 The adjusted velocity field described above during both the MoorSPICE and Pandora cruises is  
349 estimated so that conservation requirements on mass, heat, salt are met over the whole water  
350 column. Vertical advective ( $w$ ) and diffusive ( $\kappa_z$ ) exchanges are allowed between isopycnal  
351 layers, which were chosen to have a relatively homogeneous thickness over the basin, as well as  
352 freshwater and Ekman fluxes (see Germaineaud et al., 2016 for further detail). For the Pandora  
353 cruise, where silicate data is available, silicate content is conserved from the surface down to the  
354 deepest layers but not within individual layers, as it is expected to be nearly conservative within  
355 a top-to-bottom oceanic volume enclosed by hydrographic transects (Ganachaud and Wunsch,  
356 2002).

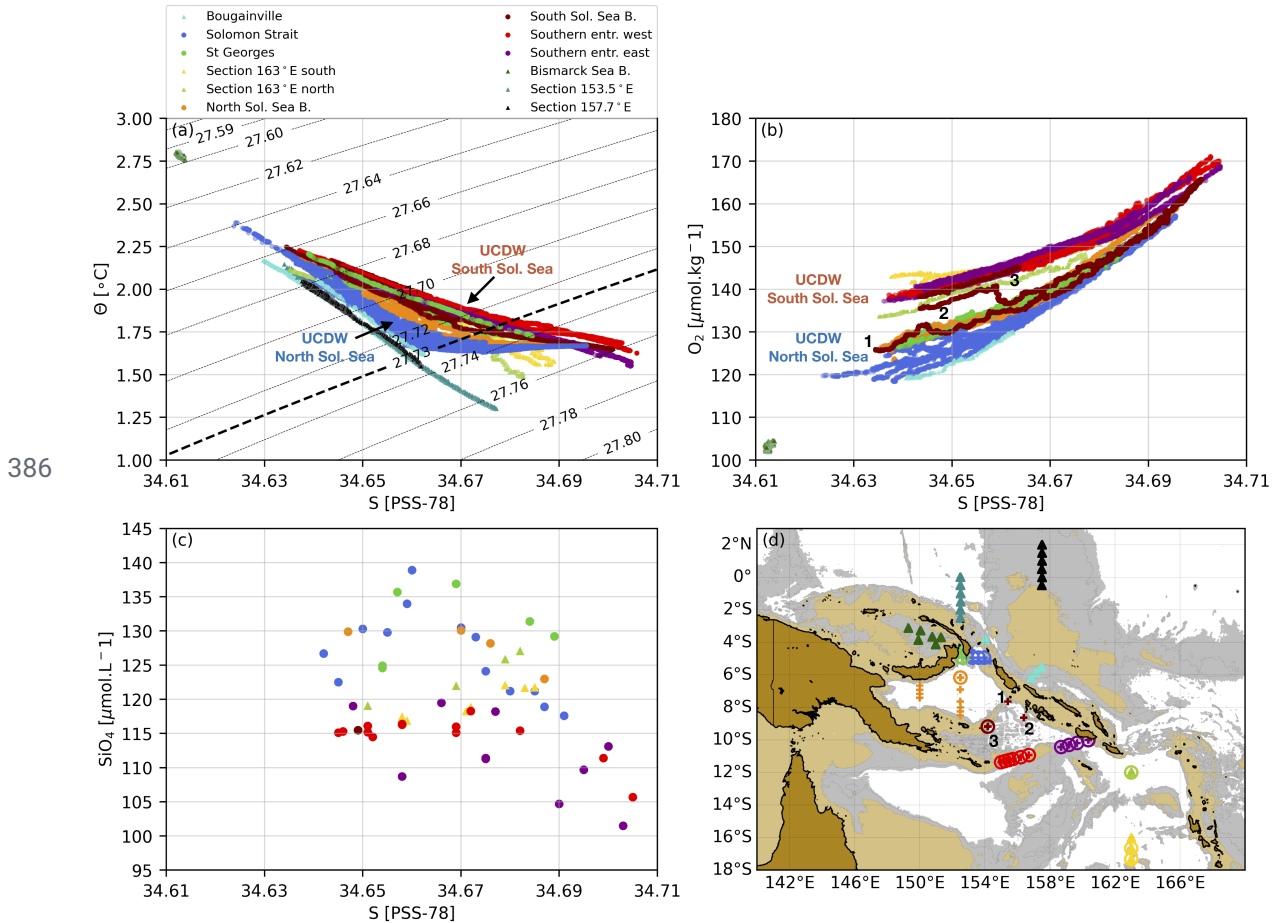
357 For both the Pandora and MoorSPICE cruises, *a priori* uncertainties of mass are set following  
358 Germaineaud et al., (2016), with larger uncertainties ( $\pm 2$  Sv instead of  $\pm 1$  Sv) near the surface  
359 and in the deepest layer, allowing exchanges with abyssal waters ( $\sigma_0 > 27.76$ ). Heat and salt are  
360 also not conserved in the surface and deepest layers, using anomaly equations and associated  
361 scaling factors (following Ganachaud, 2003). All constraints were met within uncertainties, and  
362 the estimated velocities adjusted to the deep reference level are below the initial velocity range  
363  $\pm 5$  cm s<sup>-1</sup>. Even though both adjusted model solutions allow us to infer the circulation in the  
364 Solomon Sea at fairly high vertical resolution, it should be noted that their weaknesses include  
365 the assumption that the cruise data collectively provide a synoptic snapshot and possible bias is  
366 introduced by the data-based constraints used to adjust the initial guess through the inversion.

## 367 **4 Deep water distributions in the Solomon Sea**

### 368 **4.1 Water mass properties**

369 The deep waters properties are first investigated inside the Solomon and Bismarck Seas for  
370 waters between 2000 and 3500 m, corresponding to potential densities below  $\sigma_0 = 27.59$  and  
371 above  $\sigma_0 = 27.78$  (Fig. 3a). North of 25°S in the Southwest Pacific Basin to 15°N in the Central  
372 Pacific Basin, UCDW exhibits relatively low-O<sub>2</sub> (130-150  $\mu\text{mol.kg}^{-1}$ ) with  $\theta$  and S values ranging  
373 from 1.2° to 2.2°C and 34.64-34.7, respectively over the 2000-3500 m depth range (see Table 1).  
374 During the two SPICE cruises, corresponding UCDW properties are found in the Solomon Sea  
375 Basin, although there is a marked difference between the stations located in the northern part of  
376 the basin and those at the southern entrance. A distinction must also be made for waters with  
377 potential densities above  $\sigma_0 = 27.73$  ( $\sim 2600$  m depth; bold dashed line in Fig. 3a), corresponding  
378 to the sill depth near Solomon Strait. To the north, within Solomon Strait (blue dots in Fig. 3),  
379 UCDW lighter than  $\sigma_0 = 27.73$  is colder (blue dots in Fig. 3a), less oxygenated (Fig. 3b) and

380  $\text{SiO}_4$ -richer (Fig. 3c) than that at the southern entrance (red dots) and within the South Solomon  
 381 Trench (magenta dots). The water properties at these depths in Solomon Strait are similar to  
 382 those observed along the northern transects carried out at 153.5°E (green dots) and 157.7°E  
 383 (black dots) during Cassiopée, indicating possible interbasin exchanges between the East  
 384 Caroline Basin and the Solomon Sea Basin (at least in the northern part) below 2000 m and  
 385 above the sill depth.

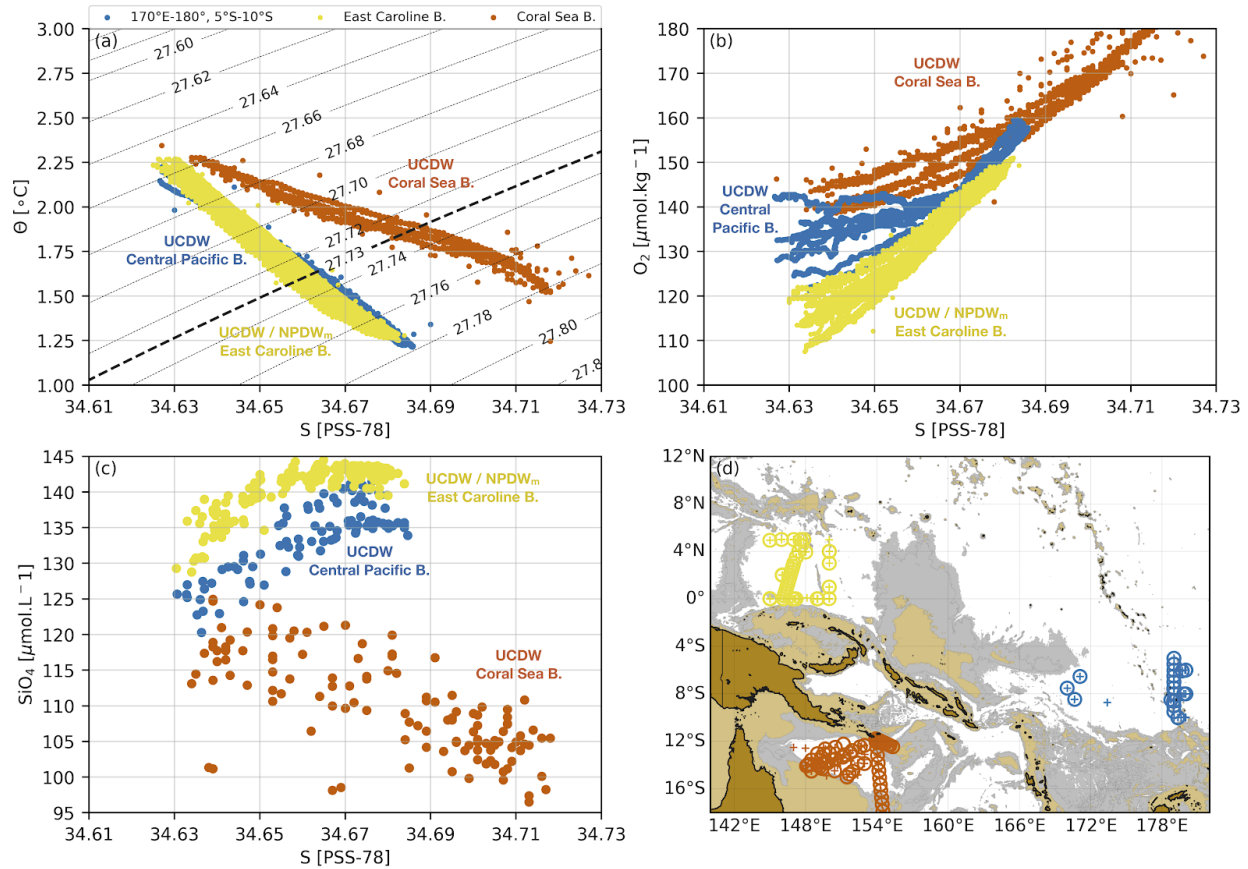


387 **Fig. 3:** Water mass property plots for measurements collected at depths between 2000 to 3500 m during  
 388 the SPICE cruises and the Cassiopée cruise. (a) Potential temperature-salinity  $\theta$ -S; bold dashed indicates  
 389 the  $\sigma_0$  level above which the East Caroline Basin and the Solomon Sea Basin remain connected, (b)  
 390 dissolved oxygen-salinity  $\text{O}_2$ -S and (c) silicate-salinity  $\text{SiO}_4$ -S diagrams. Colors correspond to the  
 391 locations as indicated in legend (top) in (a). The southern and northern origins of UCDW are also  
 392 indicated; Sol. = Solomon; B. = Basin and entr. = entrance. Hydrographic stations are shown in (d), where  
 393 colored crosses indicate the CTD- $\text{O}_2$  casts, and colored circles indicate the bottle water samples. Note that  
 394 the CTD- $\text{O}_2$  casts outside the Solomon Sea are shown as triangles instead of dots. The stations associated  
 395 with the numbered  $\text{O}_2$ -S curves in (b) are indicated in (d). Light brown shading shows bathymetry above  
 396 2000 m, and gray shading indicates areas at depths of 2000 to 3500 m, as in Fig. 1.

397 Inside the northern part of the Solomon Sea, including near Vitiaz Strait and St George's  
398 Channel, waters appear to be a mixture between waters in Solomon Strait and waters entering  
399 from the south. This view is contrary to the tracer study of Sokolov and Rintoul (2000), although  
400 as mentioned before, only sparse observations of  $\theta$  and  $S$  were available at the time of their  
401 study. During Pandora, the  $O_2$  distributions along the transect at  $163^\circ\text{E}$  show similarly high- $O_2$   
402 values to those found at the southern entrance of the Solomon Sea. This suggests that UCDW  
403 entering from the north through Solomon Strait is older than the UCDW entering the Solomon  
404 Sea from the south. Below  $\sigma_0 = 27.73$ , waters properties in the whole Solomon Sea Basin tend to  
405 have more consistent properties in  $\theta$  and  $S$  as we go deeper in the water column, suggesting a  
406 unique origin. Yet, UCDW is slightly less oxygenated and  $\text{SiO}_4$ -richer in the northern part than at  
407 the southern entrance, suggesting older water, and a slower ventilation inside the basin. The  
408 evolution of the  $O_2$ - $S$  curves within the southern part of the Solomon Sea (brown dots in Fig. 3b)  
409 further show that UCDW flowing there comes from the southern entrance, although some  
410 differences in property values are noted (see the numbered  $O_2$ - $S$  curves and their respective  
411 locations in Figs. 3b, d). It also appears that an inflow of UCDW into the northern part of the  
412 basin is somewhat limited below  $\sigma_0 = 27.72$  ( $\sim 2400$  m), i.e. the potential density at which a  
413 seesaw in  $O_2$  near  $S = 34.66$  is observed in the  $O_2$ - $S$  curve numbered as 2 in Fig. 3b.

414 To investigate the different sources of UCDW into the Solomon Sea Basin, we use WOA18  
415 property distributions (Fig. 4) at depths between 2000 to 3500 m for three possible origin  
416 regions: the Coral Sea Basin south of Papua New Guinea (orange dots in Fig. 4), east of the  
417 Solomon Sea in the Central Pacific Basin ( $170^\circ\text{E}$ - $180^\circ$ ,  $5^\circ\text{S}$ - $10^\circ\text{S}$ ; blue dots in Fig. 4) and the  
418 East Caroline Basin (yellow dots in Fig. 4). While UCDW is warmer (Fig. 4a), more  $O_2$ -rich  
419 (Fig. 4b) and  $\text{SiO}_4$ -poor (Fig. 4c) in the Coral Sea Basin than that found in the Central Pacific, it  
420 has similar water property values to the UCDW found at the southern entrance of the Solomon  
421 Sea. This indicates that most of the UCDW entering the Solomon Sea Basin in the south comes  
422 primarily from the Coral Sea Basin rather than the Central Pacific Basin. This is consistent with  
423 the initial suggestion by Wyrтки (1961), but *a priori* not consistent with conclusions by Sokolov  
424 and Rintoul (2000). The latter authors concluded that waters entering the Solomon Sea (via the  
425 South Solomon Trench) mostly originated from the Central Pacific. Here, our results suggest that  
426 waters in the South Solomon Trench have properties similar to those in the Coral Sea Basin, and  
427 thus most likely originate from the Coral Sea Basin.





428

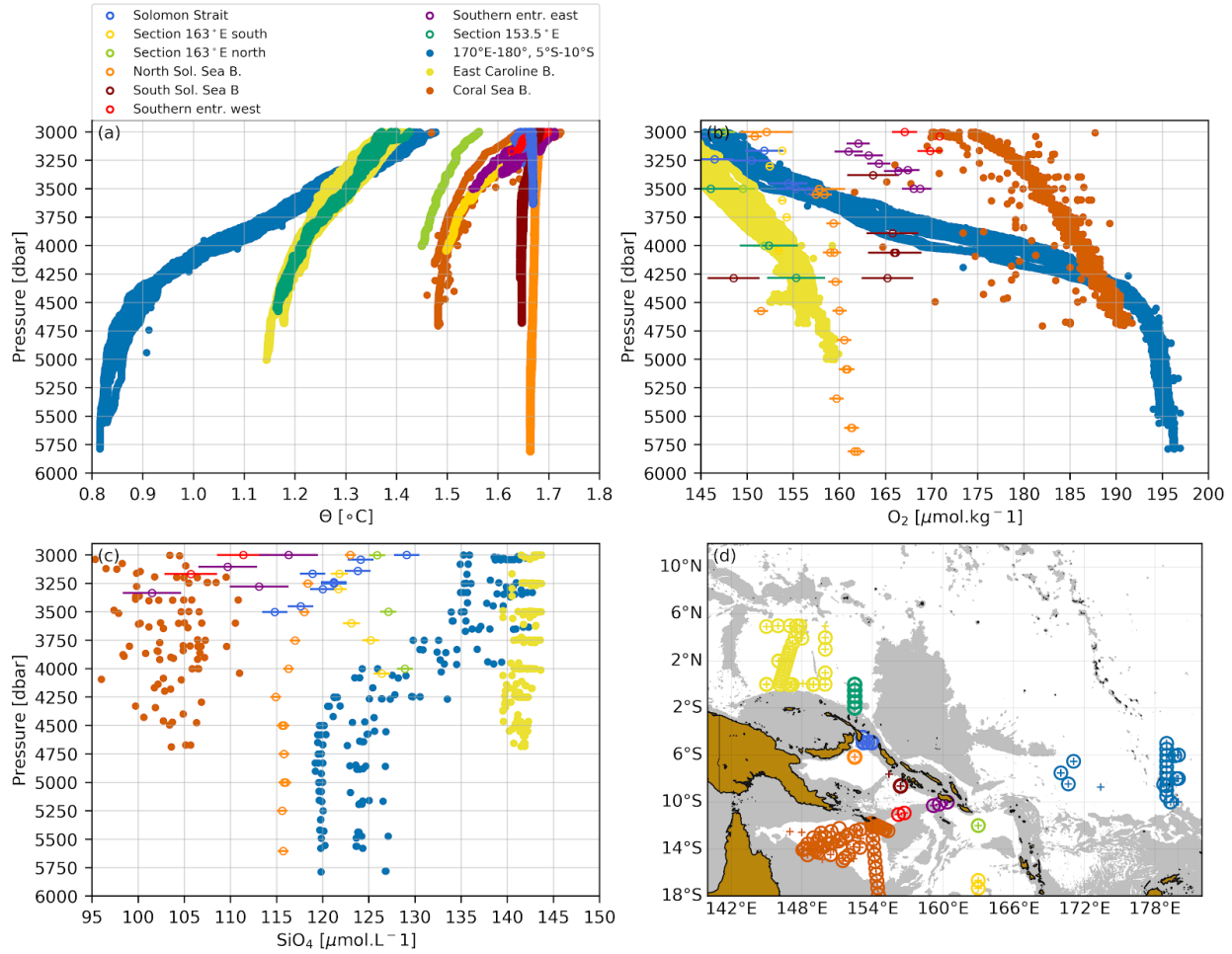
429 **Fig. 4:** Historical water mass property plots from WOA18 at depths between 2000 to 3500 m. (a)  
 430 Potential temperature-salinity  $\theta$ -S; bold dashed indicates the potential density anomaly  $\sigma_0$  ( $kg\ m^{-3}$ ;  
 431 referenced to a sea pressure of zero dbar) level above which the East Caroline Basin and the Solomon Sea  
 432 Basin remain connected, as in Fig. 3, (b) dissolved oxygen-salinity  $O_2$ -S and (c) silicate-salinity  $SiO_4$ -S  
 433 diagrams. Colors correspond to the locations as indicated in legend (top) in (a). The deep water masses  
 434 and origin are also indicated; B. = Basin. Hydrographic stations are shown in (d), where colored crosses  
 435 indicate the CTD- $O_2$  casts and colored circles indicate the bottle water samples. Light brown shading  
 436 shows bathymetry above 2000 m, and gray shading indicates areas at depths of 2000 to 3500 m, as in Fig.  
 437 1.

438 North, in the East Caroline Basin, we recognize a region of cold water (Fig. 4a), depleted in  $O_2$   
 439 (Fig. 4b) and enriched in  $SiO_4$  (Fig. 4c), indicating an  $NPDW_m$  flow that most likely emanates  
 440 from the neighboring East Mariana Basin located further north (where both basins remain  
 441 connected above 4200-4300 m). Previous studies (e.g., Johnson et al., 1993; Siedler et al., 2004)  
 442 have identified southward transports of  $NPDW_m$  across the East Mariana Basin, suggesting that  
 443 the East Caroline Basin is a region where UCDW and  $NPDW_m$  mix; or at least, where incursions  
 444 of  $NPDW_m$  into the basin reinforce the low- $O_2$  and high- $SiO_4$  characteristic of the aged UCDW  
 445 observed in that region. Finally, it is important to note that within the Bismarck Sea Basin (see  
 446 Fig. 2 for location), which is no deeper than 2500 m, we do not observe (based on MoorSPICE

447 data) any water mass properties corresponding to either UCDW or NPDW<sub>m</sub>. Based on Figs. 3a  
448 and 3b, the basin appears to be totally closed below 2000 m and exhibits completely  
449 homogeneous waters at all depths below 2000 m, which consist of warmer, fresher, and more  
450 O<sub>2</sub>-poor water (cluster of dark green dots near S = 34.61 in Figs. 3a and 3b) than the deep waters  
451 encountered in the East Caroline and Solomon Sea Basins. The distributions of  $\theta$  (Fig. S2a) and  
452 S (Fig. S2b) in the Bismarck Sea Basin at depths between 1000 to 1500 m are similar to those  
453 found in St George's Channel and Solomon Strait, while waters below 1750 m are vertically  
454 homogeneous throughout the Bismarck Sea Basin. It is thus clear that the Bismarck Sea Basin  
455 (which is in fact enclosed below 1750 m) is isolated from the deep circulation in the western  
456 equatorial Pacific at UCDW levels. Interestingly, the oxygen (Fig. S2c) remains constant with  
457 depth from 1750 to 2500 m, despite the lack of ventilation, while the nutrients (not shown)  
458 remain almost constant. While a detailed investigation of this constant pattern in both oxygen  
459 and nutrients is beyond the scope of this study, this suggests either that there is no oxygen  
460 consumption (remineralization) at depth, or that remineralization is compensated by downward  
461 diffusion of oxygen toward the deep ocean.

462 The deep water properties are further investigated for waters below 3500 m (Fig. 5),  
463 corresponding to potential densities below  $\sigma_0 = 27.78$ . In Fig. 5, the property values identifying  
464 the upper boundary of LCDW in the East Caroline Basin (i.e.,  $\theta < 1.2^\circ\text{C}$ , S = 34.685, O<sub>2</sub> = 155  
465  $\mu\text{mol.kg}^{-1}$  and SiO<sub>4</sub> > 140  $\mu\text{mol.kg}^{-1}$ ; yellow dots) are found at depths below 4000 m, confirming  
466 similar conclusions by Seidler et al. (2004). From there, shallow topography prevents LCDW  
467 from proceeding westward into the West Caroline Basin and southward into the Solomon Sea  
468 Basin, as the East Caroline Basin is closed to the west and to the south below 3500 m. As no  
469 northern source exists for the bottom water in the Solomon Sea Basin, the densest water, that  
470 may originate as the lightest portion of LCDW, has to arrive from the south. In the Central  
471 Pacific Basin region (170°E-180°, 5°S-10°S; blue dots), water mass indicators marking the  
472 boundary between UCDW and LCDW are found at about 3750-4000 m, where  $\theta < 1.2^\circ\text{C}$  (Fig.  
473 5a) is associated with a pattern of increasing O<sub>2</sub> (Fig. 5b) and decreasing SiO<sub>4</sub> (Fig. 5c). As  
474 expected, the LCDW at the western edge of the Central Pacific is more O<sub>2</sub>-rich and SiO<sub>4</sub>-poor  
475 than that found in the East Caroline Basin at those depths, reflecting the northward motion (and  
476 the aging) of LCDW there. Note that a LCDW inflow directly from the Central Pacific Basin  
477 into the Solomon Sea is expected to be blocked by topography, as the deepest narrow passages  
478 through the Solomon Islands do not exceed 3500 m depth.

479



480 **Fig. 5:** (a-c) Vertical profiles with pressure (dbar) of potential temperature  $\theta$  ( $^{\circ}\text{C}$ ; referenced to a sea  
 481 pressure of zero dbar) in (a), dissolved oxygen  $\text{O}_2$  ( $\mu\text{mol.kg}^{-1}$ ) in (b) and silicate  $\text{SiO}_4$  ( $\mu\text{mol.kg}^{-1}$ ) in (c)  
 482 from measurements collected at depths greater than 3000 m during the two SPICE cruises and Cassiopée  
 483 (colored circles), and WOA18 (colored dots). Error bars associated with  $\text{O}_2$  (b) and  $\text{SiO}_4$  (c) from the  
 484 SPICE cruises and Cassiopée were constructed from the standard error of the mean for each depth profile.  
 485 Colors correspond to the locations as indicated in legend (top); Sol. = Solomon and B. = Basin and entr. =  
 486 entrance. Hydrographic stations are shown in (d), where colored crosses indicate the CTD- $\text{O}_2$  casts, and  
 487 colored circles indicate the bottle water samples. Gray shading indicates areas at depths greater than 3000  
 488 m.

489 Below 3500 m, we find  $\theta$  values between  $1.6^{\circ}$  to  $1.7^{\circ}\text{C}$  at the deep stations occupied inside the  
 490 southern and northern parts of the Solomon Sea Basin (see Fig. 5d for locations). These waters  
 491 are warmer than all possible sources at the same depths. Waters in the Coral Sea Basin exhibit  $\theta$   
 492 values from  $1.45^{\circ}$  to  $1.55^{\circ}\text{C}$ , consistent with observations from Wyrтки (1961) and Sokolov and  
 493 Rintoul (2000), who found  $\theta = 1.46^{\circ}\text{C}$  for the deep waters in the Coral Sea Basin. Farther east, in  
 494 the Central Pacific Basin, deep waters are much cooler ( $\theta < 1.3^{\circ}\text{C}$ ). Several geothermal sources  
 495 have been reported in the region (e.g., Halunen and von Herzen, 1973; Joshima and Honza,

496 1986), with a mean heat flow of about  $85 \text{ mW}\cdot\text{m}^{-2}$  in the Solomon Sea Basin. However, note that  
497 heating the water column over at least 1000 m above the seafloor by  $0.15^\circ\text{C}$  (assuming a  
498 constant heat flux of  $85 \text{ mW}\cdot\text{m}^{-2}$ ) would imply no water motion in the abyssal layer for about 530  
499 years, which is unrealistic. As a geothermal source inside the Solomon Sea Basin able to heat  
500 waters at such great depths is not possible, this indicates that only the densest part of UCDW  
501 (i.e., above 3500 m depth and  $\sigma_0 = 27.78$ ) can fill the deepest part of the basin. The  $\text{O}_2$  (Fig. 5b),  
502  $\text{SiO}_4$  (Fig. 5c) and S (Fig. S3a) distributions also confirm these conclusions, although the values  
503 of  $\text{O}_2$  in the Coral Sea Basin and the Central Pacific Basin are close to each other at depths  
504 between 3750 to 4750 m.

505 In the Solomon Sea Basin, for each cruise we observe nearly vertically uniform  $\theta$  and S from  
506 3500 m to the near-bottom depth, which may reflect strong diapycnal exchanges at those depths  
507 and/or long residence times for those water masses in the basin. Furthermore, only minor  
508 changes of  $\theta$  ( $< 0.05^\circ\text{C}$ ; Fig. 5a) and  $\text{O}_2$  ( $< 1.5 \mu\text{mol}\cdot\text{kg}^{-1}$ ; Fig. 5b) are found between the  
509 common stations from Pandora and MoorSPICE obtained during contrasting seasons, ruling out  
510 the possibility of significant seasonal variability. Corresponding changes in S can reach values of  
511 about 0.01 PSS-78 (Fig. S3a), with consistently higher S during MoorSPICE than found during  
512 Pandora. It is unclear though whether these observed salinity shifts reflect actual salinity  
513 variations or are calibration differences in conductivity sensors between both cruises, although  
514 comparisons of CTD S with bottle S were mostly within the manufacturer's accuracy  
515 specifications of the S sensor ( $< 0.003$  PSS-78). Either way, it appears that deep waters are  
516 vertically homogenized below 3500 m in the northern part of the Solomon Sea Basin, as  
517 confirmed by the vertical (and homogeneous) potential density profiles displayed in Fig. S4a.

518 A thorough analysis of the bottom topography in the Solomon Sea area (not shown) reveals that  
519 exchanges at depths reaching 3900 m are possible between the Coral Sea Basin and the southern  
520 Solomon Sea Basin via a deep narrow channel (known as the Pocklington Trough) located at the  
521 western end of the southern entrance (see Fig. 2 for location). Exchanges are also possible via the  
522 Solomon Sea Trough at the eastern end of the southern entrance of the Solomon Sea, with sill  
523 depths of about 4000 m. Between the southern and the northern parts of the Solomon Sea Basin,  
524 a narrow passage is possible at depths reaching 4100 m. Yet, it appears that these passages are  
525 too narrow to allow a significant water mass transport below 3500 m, and so the deep waters  
526 inside the Solomon Sea are not ventilated below 3500 m. Therefore, the apparent high- $\text{O}_2$  signal  
527 mentioned above is in fact a signature of high- $\text{O}_2$  UCDW waters originating from the Coral Sea  
528 Basin. The less  $\text{O}_2$ -rich (Fig. 5b) and the higher  $\text{SiO}_4$  (Fig. 5c) characteristics in the northern part  
529 of the Solomon Sea Basin compared to the south is also an indicator of an aged inflow of dense  
530 UCDW coming from the Coral Sea Basin. In the Solomon Sea Basin, similar to the deep  
531 Bismarck Sea, it seems that there is little or no remineralization at depth, as both the oxygen and  
532 silicate remain constant locally below 3500 m.

533 **4.2 Transports, mixing and variability**

534 In the Solomon Sea box as defined by the sections across the inflow and outflow regions  
 535 measured during the two SPICE cruises (Fig. 2), there is an adjusted transport needed across the  
 536 southern section during the inversion. Most of the UCDW enters the box via two passages, a  
 537 westward component between 156°E-157°E and one further east at 159°E-160°E between  
 538 isopycnals ranging from 27.65 (~ 2000 m) to 27.76 (~ 3250 m)  $\sigma_\theta$ . For Pandora an adjustment of  
 539 about  $2.3 \pm 1.7$  Sv of UCDW across the southern transect is needed (Table 2). This equatorward  
 540 adjusted transport of UCDW is halved during MoorSPICE ( $1.2 \pm 0.7$  Sv), possibly due to  
 541 unaccounted net transport across the southern transect because CTD casts were shallower there  
 542 during MoorSPICE compared to during Pandora. At the northern end of the Solomon Sea, the  
 543 adjusted transport of UCDW across the transect joining St George's Channel and Solomon Strait  
 544 amounts to  $1.6 \pm 1.7$  Sv for Pandora and  $1.4 \pm 1.3$  Sv for MoorSPICE (Table 2). The large  
 545 uncertainty associated with these estimates suggests that transport could be either in or out of the  
 546 basin, or rather close to zero at the UCDW levels. As noted before, the sill depth of St. George's  
 547 Channel is 1400 m, and the sill depth out of Solomon Strait is 2600 m, implying that the  
 548 transports below 2600 m are in fact necessarily zero.

Upper ( $\sigma_\theta$ , kg.m <sup>-3</sup> )	Lower ( $\sigma_\theta$ , kg.m <sup>-3</sup> )	Southern entrance	St George's-Solomon
27.65 (~ 2000 m)	27.76 (~ 3250 m)	<b>Before inversion</b> <b>Pandora: 1.6</b> <b>MoorSPICE: -0.1</b> <hr/> <b>After inversion</b> <b>Pandora: <math>2.3 \pm 1.7</math></b> <b>MoorSPICE: <math>1.2 \pm 0.7</math></b>	<b>Before inversion</b> <b>Pandora: 1.1</b> <b>MoorSPICE: -1.8</b> <hr/> <b>After inversion</b> <b>Pandora: <math>1.6 \pm 1.7</math></b> <b>MoorSPICE: <math>1.4 \pm 1.3</math></b>

549 **Table 2:** Boundaries of the upper and lower ranges defining the deep waters and corresponding volume  
 550 transports (Sv;  $1 \text{ Sv} \equiv 10^6 \text{ m}^3 \text{ s}^{-1}$ ) during the Pandora and MoorSPICE cruises. Positive values indicate  
 551 equatorward flow, negative values are southward and uncertainties are one standard deviation. After  
 552 inversion transport estimates in and out the box are not exactly similar ( $2.3$  vs.  $1.6$  Sv,  $1.2$  vs.  $1.4$  Sv), due  
 553 to diapycnal fluxes to surrounding layers and residual noise.

554 Based on the assumption of synopticity of the measurements, the inverse-derived adjusted  
 555 transports provide reliable estimates within errors, but it is useful to compare with the initial  
 556 (nonadjusted) transports. At the southern entrance, the nonadjusted transport of UCDW is  $1.6$  Sv  
 557 during Pandora and nearly zero during MoorSPICE, which is consistent with the model results  
 558 (within errors) given above. Both nonadjusted and adjusted transports during Pandora confirm  
 559 that UCDW can enter the Solomon Sea through the southern entrance, although this inflow of

560 UCDW might not be a persistent transport pattern based on the MoorSPICE transport estimates.  
561 At the northeastern exit of the Solomon Sea, we find nonadjusted UCDW transports of 1.1 Sv  
562 and -1.8 Sv during Pandora and MoorSPICE, respectively. This is consistent with a pattern of  
563 transports in and out of the Solomon Sea Basin above its sill depth ( $\sim 2600$  m); nevertheless, the  
564 nonadjusted transports during MoorSPICE do not agree with that adjusted through inversion.  
565 One possible explanation for this discrepancy may be that, in our model set up with MoorSPICE  
566 data, we find quite large vertical velocities ( $w > 1 \times 10^{-4}$  cm.s<sup>-1</sup>) across the isopycnals at 27.65 ( $\sim$   
567 2000 m) to 27.71 ( $\sim 2500$  m)  $\sigma_0$ , indicating the upward transfer of deep water at these densities.

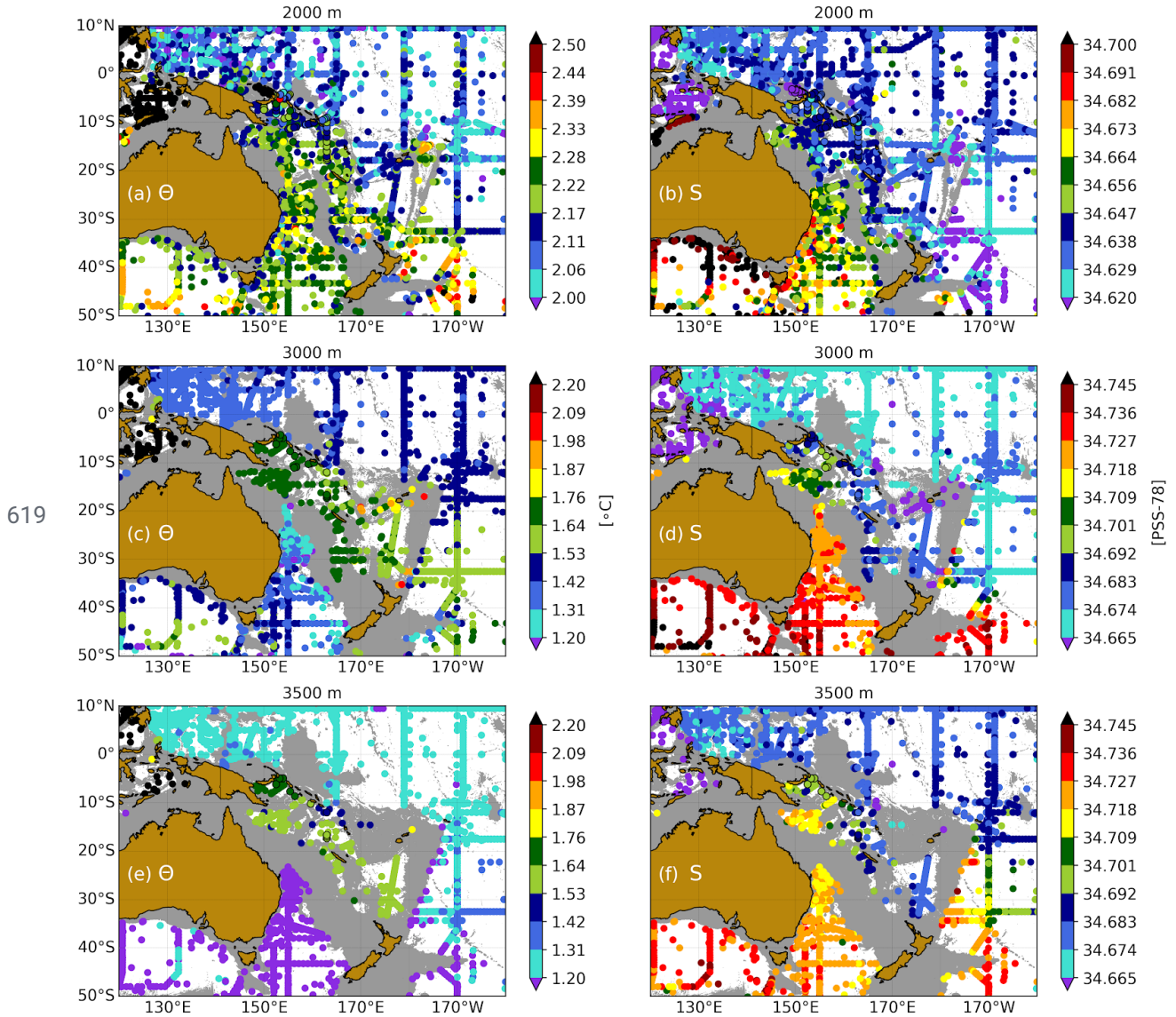
568 In Albery et al. (2019), the mean transport through Solomon Strait derived from the SPICE  
569 mooring deployment over July 2012 to March 2014 was estimated at  $4.6 \pm 1.0$  Sv **into** the  
570 Solomon Sea from 1500 to 2500 m (27.50-27.71  $\sigma_0$ ). During the two SPICE cruises, both the  
571 nonadjusted and adjusted transports in the same potential density range (Table S1) indicate an  
572 opposite transport pattern (i.e., out of the Solomon Sea Basin) to that determined from the  
573 moored observations. The inflow inside the Solomon Sea was mainly found from a mooring  
574 deployed in the eastern part of the Solomon Strait (Albery et al., 2019). The total transport  
575 estimate is possibly biased, as the velocities deeper than 1700 m were extrapolated down to 2500  
576 m, and also extrapolated across the Strait (see Albery et al., 2019 for further detail). Yet, these  
577 mooring data provide clear evidence for a persistent throughflow from the East Caroline Basin  
578 into the Solomon Sea Basin below 1500 m. This inflow is fully consistent with our conclusions  
579 from hydrological properties suggesting the existence of an intrusion of waters through Solomon  
580 Strait above  $\sigma_0 = 27.73$  (see section 4.1). Below, in the potential density layer 27.71-27.76  $\sigma_0$ ,  
581 rather small transports ( $\sim 1$  Sv; Table S1) are also out of the basin during Pandora, while larger  
582 transports (3-5 Sv; Table S1) are into the basin during MoorSPICE. The differences in transports  
583 through Solomon Strait are surprising, but they might reflect variations in layer thickness of the  
584 deep flow there, associated with significant diapycnal exchanges.

585 Our model provides layer-to-layer estimates of diffusivity  $\kappa_z$ , however, the obtained diffusion  
586 coefficients are not accurate enough (because of too large uncertainties) to draw any conclusion  
587 on mixing processes. To gain further insight on mixing in the deep layers of the Solomon Sea,  
588 diffusivity can also be inferred using finescale parameterization methods (e.g., Kunze et al.,  
589 2006; Polzin et al., 2014). Following the approach of Albery et al. (2017), we use 320 m long  
590 segments of CTD potential density data (from the Pandora and MoorSPICE cruises) to quantify  
591 strain variance, which is used to estimate dissipation of kinetic energy ( $\epsilon$ ), which in turn, is used  
592 to calculate strain-based estimates of  $\kappa_z$  (Fig. S5). Note that only the CTD casts carried out  
593 during the two SPICE cruises at depths greater than 3000 m within the Solomon Sea Basin are  
594 considered here. For each segment, the mean squared buoyancy frequency ( $N^2$ ) is also calculated  
595 and estimates of both  $\epsilon$  and  $N^2$  from the considered casts (all greater than 3000 m) are bin  
596 averaged in 320 m bins over the 2000-4880 m depth range. Average diffusivity  $\kappa_z = \gamma \frac{\epsilon}{N^2}$ , is then

597 estimated using the bin averaged  $\epsilon$  and  $N^2$ , with an empirical mixing efficiency  $\gamma$  of 0.2 (based on  
598 Peltier and Caulfield, 2003). The mean profile of  $\kappa_z$  (Fig. S5) is maximum near 2500 m at  $5 \times$   
599  $10^{-4} \text{ m}^2 \text{ s}^{-1}$  and the lowest  $\kappa_z$  values ( $1-2 \times 10^{-6} \text{ m}^2 \text{ s}^{-1}$ ) occur at depths below 3750 m. Even though  
600 the error bars of  $\kappa_z$  (grey shading in Fig. S5) are large, these density-derived estimates of  $\kappa_z$   
601 further suggest that diapycnal mixing may play a key role in the transport variability (via layer  
602 thickness changes) observed at Solomon Strait between 1500 m to its sill depth near 2600 m.

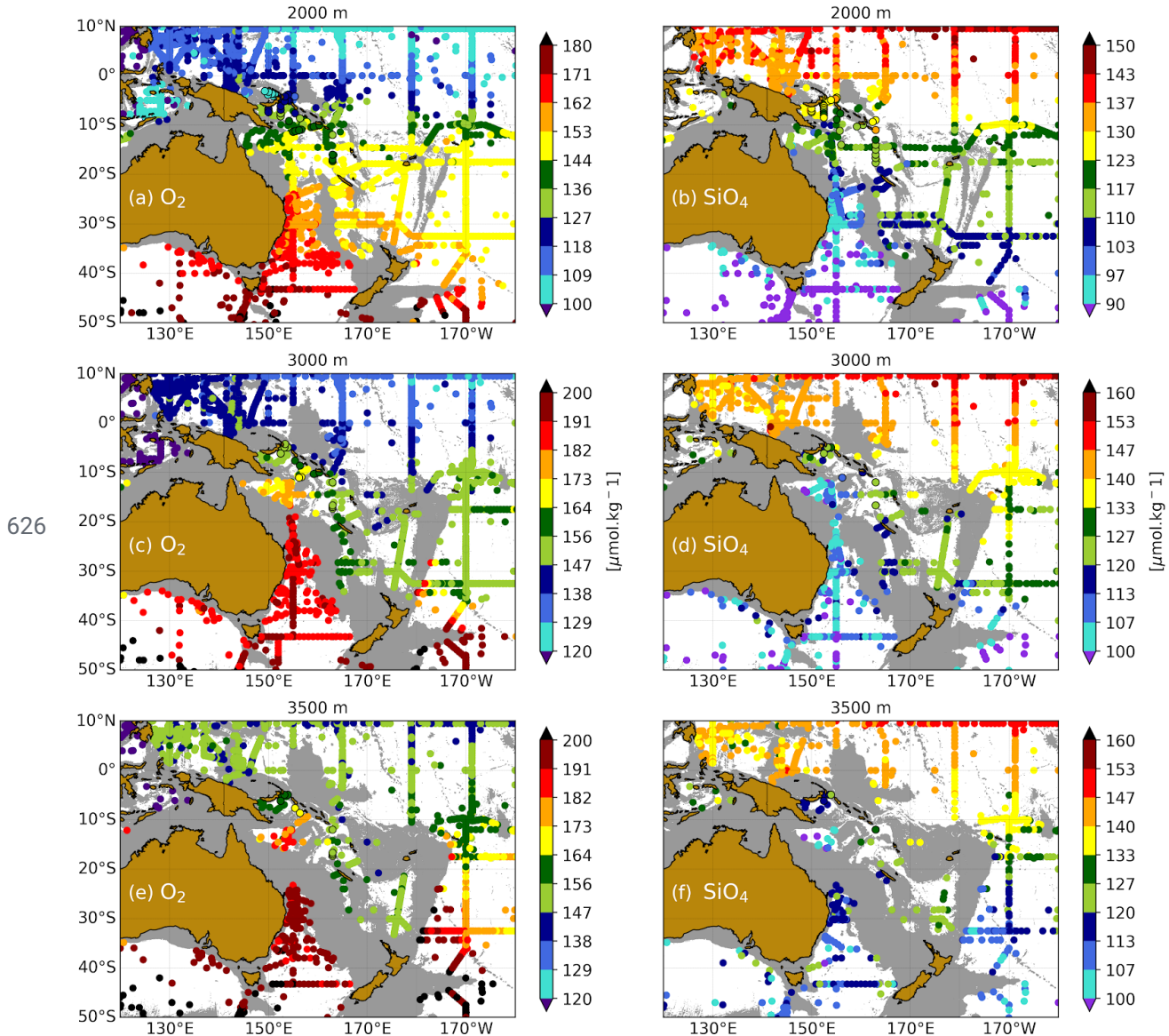
### 603 **5 Connection to the Pacific circulation**

604 At 2000 m depth, the historical measurements of  $\theta$  (Fig. 6a), S (Fig. 6b),  $\text{O}_2$  (Fig. 7a) and  $\text{SiO}_4$   
605 (Fig. 7b) combined with the corresponding observations from the two SPICE cruises give a  
606 consistent picture for the lightest UCDW flow between  $20^\circ\text{S}$  to  $10^\circ\text{N}$ . There is a region of  
607 high- $\text{O}_2$  ( $> 140 \mu\text{mol.kg}^{-1}$ ), low- $\text{SiO}_4$  ( $< 130 \mu\text{mol.kg}^{-1}$ ), low- $\theta$  and relatively low-S at the  
608 southern entrance of the Solomon Sea traced from the Coral Sea Basin. These distinct property  
609 distributions can also be traced from the New Caledonia Trough, the New Hebrides Basin and  
610 the South Fiji Basin in the southeastern part of the Coral Sea. The South Fiji Basin is connected  
611 with the Southwest Pacific Basin via narrow passages at the southern tip of the Tonga-Kermadec  
612 Ridge, it is therefore possible that the lightest part of UCDW is also exchanged through these  
613 passages between both basins in the potential density range  $27.65-27.69 \sigma_0$  (Fig. S6a), before  
614 proceeding equatorward. Further north, the water properties of aged UCDW (more  $\text{O}_2$ -poor and  
615  $\text{SiO}_4$ -rich than the UCDW south of  $10^\circ\text{S}$ ) are clearly identified in the East Caroline Basin and the  
616 northern part of the Solomon Sea Basin. As discussed in section 4, waters at these depths in the  
617 Solomon Sea are a mixture between Coral Sea waters entering from the southern entrance and  
618 waters from the East Caroline Basin entering the Solomon Sea through Solomon Strait.



619 **Fig. 6:** Historical measurements (colored dots) of (a, c, e) potential temperature  $\theta$  ( $^{\circ}\text{C}$ ; referred to a sea  
 621 pressure of zero dbar) and (b, d, f) salinity  $S$  (PSS-78) from WOA18 at three depth levels encompassing  
 622 the UCDW, overlaid by the corresponding tracers measured during the two SPICE cruises (colored dots  
 623 with black outlines). (a, b) show  $\theta$  and  $S$  distributions at 2000 m depth, while (c, d) show similar  
 624 distributions at 3000 m and (e, f) at 3500 m. In each panel, areas shallower than each corresponding depth  
 625 level are shaded in gray.





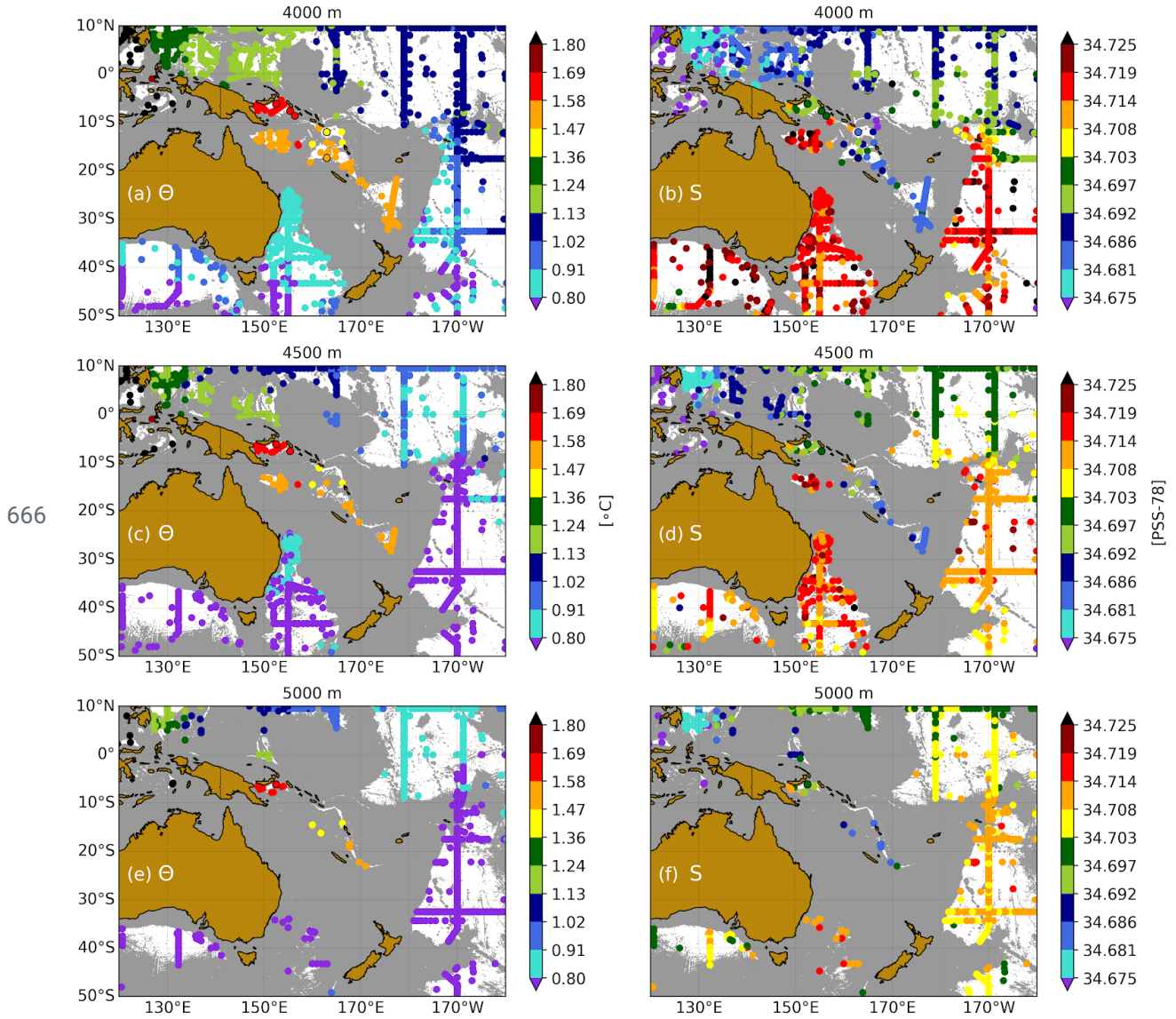
627 **Fig. 7:** Historical measurements (colored dots) of (a, c, e) dissolved oxygen  $O_2$  ( $\mu\text{mol.kg}^{-1}$ ) and (b, d, f)  
 628 silicate  $SiO_4$  ( $\mu\text{mol.kg}^{-1}$ ) from WOA18 at three depth levels encompassing the UCDW, as in Fig. 6. The  
 629 corresponding tracers from the two SPICE cruises are indicated as colored dots with black outlines, and  
 630 areas shallower than each corresponding depth level are shaded in gray.

631 At 3000 m depth (Figs. 6c, d and Figs. 7c, d), an inflow of denser UCDW into the Solomon Sea  
 632 can only happen in the south, East Caroline Basin waters are blocked by topography. As  
 633 mentioned in section 4.1, UCDW coming from the Coral Sea Basin can enter the Solomon Sea  
 634 via the Pocklington Trough, while UCDW emanating from the New Hebrides and the South Fiji  
 635 Basins can enter the Solomon Sea Basin. UCDW inflow originating from the New Caledonia  
 636 Trough might also occur. The property distributions support this view, although UCDW in the  
 637 Coral Sea Basin is, for similar  $\theta$  classes (Fig. 6c), saltier (Fig. 6d), more  $O_2$ -rich (Fig. 7c) and

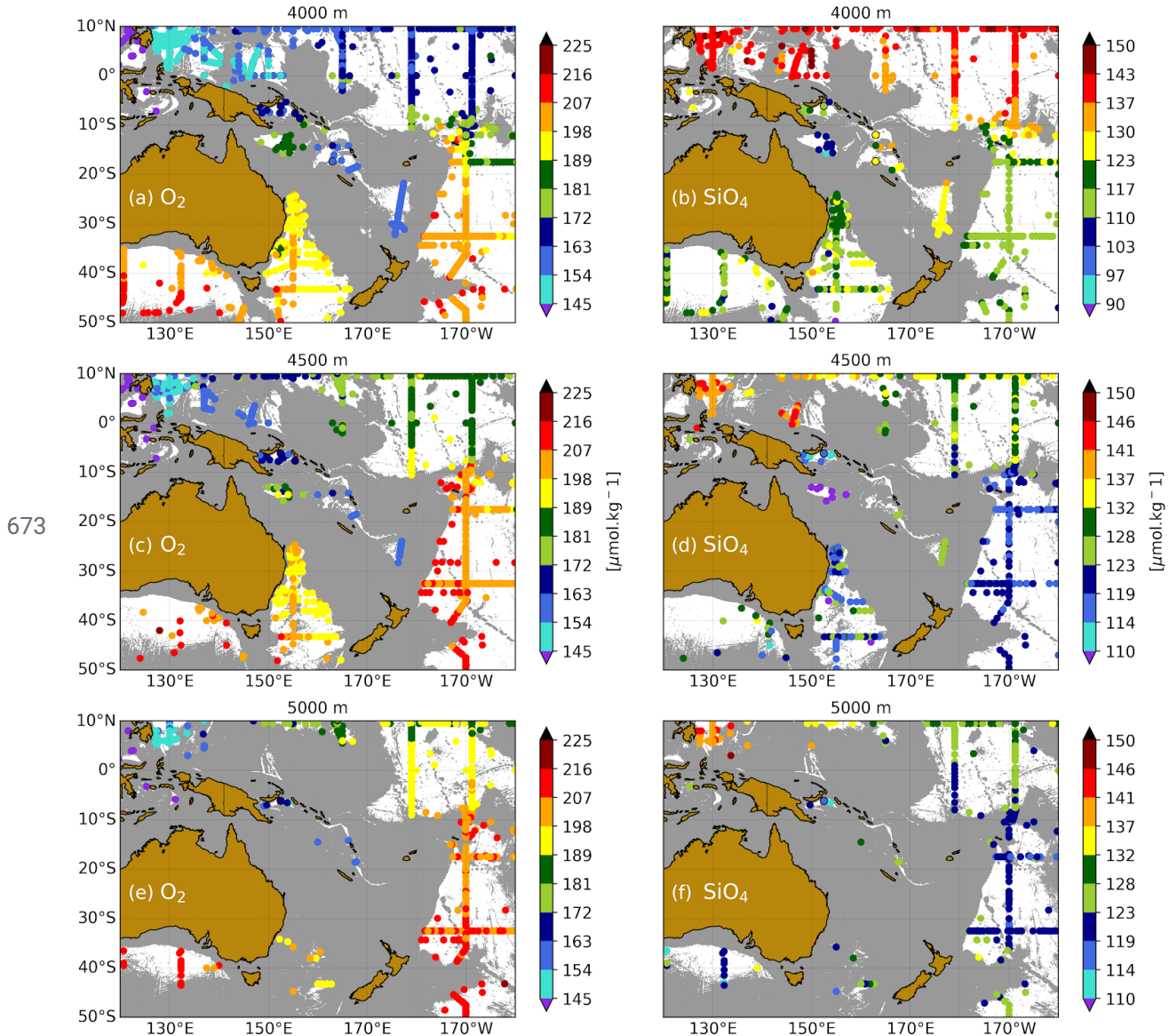
638  $\text{SiO}_4$ -poor (Fig. 7d) than UCDW originating from the New Hebrides and the South Fiji Basins.  
639 This pattern of high- $\text{O}_2$  and low- $\text{SiO}_4$  possibly reflects changes in the UCDW layer thickness  
640 (and thus diapycnal exchange), allowing an upwelling of UCDW from the East Australian Basin,  
641 which is closed to the north below 2850 m, into the Coral Sea Basin. Both UCDW from these  
642 sources flow towards each other with similar potential densities (Fig. S6b), and possibly mix  
643 around the southern entrance of the Solomon Sea before proceeding northward into the Solomon  
644 Sea. The New Caledonia Trough is closed to the north below 3000 m, while the  
645 Tonga-Kermadec Ridge prevents possible throughflow coming from the Southwest Pacific Basin  
646 (Fig. 2).

647 At 3500 m depth, the distributions of  $\theta$  (Fig. 6e), S (Fig. 6f)  $\text{O}_2$  (Fig. 7e) and  $\text{SiO}_4$  (Fig. 7f)  
648 indicate that the Solomon Sea Basin is filled by lighter UCDW coming from the Coral Sea  
649 Basin. So, even if the Solomon Sea Basin is still connected to the Coral Sea Basin via the  
650 Pocklington Trough and to the New Hebrides Basin and the South Fiji Basin via the South  
651 Solomon Trench, these passages are too narrow to allow significant transport of UCDW into the  
652 Solomon Sea, which is consistent with our findings outlined in section 4.1. Most importantly, it  
653 is clear that the apparent high- $\text{O}_2$  signature found at the deepest stations in the Solomon Sea  
654 Basin do originate from the high- $\text{O}_2$  Coral Sea waters, and extend deeper below waters with  
655 lower  $\text{O}_2$ . At 4000 m depth, the Coral Sea Basin is no longer connected to the east by the  
656 Pocklington Trough and we find, overall, similar water property distributions (Figs. 8a, b and 9a,  
657 b) than those at 3500 m from the South Fiji Basin to the Solomon Sea Basin.

658 At 4500 m depth, the southern part of the South Fiji Basin appears to be disconnected with the  
659 northwestern part of the South Pacific, and only minor changes in property values are observed  
660 (Figs. 8c, d and 9c, d). Below 4500 m, the South Fiji Basin is closed, and the circulation is  
661 strongly constrained by the sharp and complex topography over the three main trenches of the  
662 Southwest Pacific: the New Hebrides Trench east of New Caledonia, the South Solomon Trench  
663 that runs along the Solomon Islands and the New Britain Trench in the Solomon Sea. However,  
664 the question arises as to whether there is possible throughflow along this complex trench system,  
665 as only scattered measurements are available from WOA18 (Figs. 8e, f and 9e, f).



667 **Fig. 8:** Historical measurements (colored dots) of (a, c, e) potential temperature  $\theta$  ( $^{\circ}\text{C}$ ; referred to a sea  
668 pressure of zero dbar) and (b, d, f) salinity  $S$  (PSS-78) from WOA18 at three depth levels encompassing  
669 the LCDW. (a, b) show  $\theta$  and  $S$  distributions at 4000 m depth, while (c, d) show similar distributions at  
670 4500 m and (e, f) at 5000 m. The corresponding tracers from the two SPICE cruises are indicated as  
671 colored dots with black outlines, and areas shallower than each corresponding depth level are shaded in  
672 gray.



674 **Fig. 9:** Historical measurements (colored dots) of (a, c, e) dissolved oxygen  $O_2$  ( $\mu\text{mol.kg}^{-1}$ ) and (b, d, f)  
 675 silicate  $SiO_4$  ( $\mu\text{mol.kg}^{-1}$ ) from WOA18 at three depth levels encompassing the LCDW, as in Fig. 8. The  
 676 corresponding tracers from the two SPICE cruises are indicated as colored dots with black outlines, and  
 677 areas shallower than each corresponding depth level are shaded in gray.

678 The preservation of the water properties below 3500 m in these basins and trenches further  
 679 indicates that only the densest part of UCDW, which is more  $O_2$ -rich than the upper part, supplies  
 680 the bottom water in both the Coral and Solomon Seas. The potential density distributions at 3500  
 681 to 4500 m depths (Figs. S6c-f) show little regional variation, with denser water in the Coral Sea  
 682 Basin compared to that in the Solomon Sea Basin, the New Hebrides and the South Fiji Basins.  
 683 This indicates that locally in each basin, horizontal mixing processes play only a minor role in  
 684 determining the deep water mass structure, and also that the differences in  $SiO_4$  and  $O_2$  within the

685 Solomon Sea likely reflect the aging gradient of dense UCDW coming from the Coral Sea Basin,  
686 as suggested in section 4.1.

## 687 **6 Concluding remarks**

688 Our understanding of the global deep and abyssal circulation is, for the most part, still limited to  
689 scattered observations in both space and time from hydrographic sections. In the Subtropical  
690 Pacific, the deep water mass distributions are well-known to be mostly influenced by the UCDW  
691 at depths between 2000 to 3500 m, while below, a pattern of higher S, lower SiO<sub>4</sub> and increasing  
692 values of O<sub>2</sub> indicates the influence of the LCDW. However, the presence and fate of both water  
693 masses in the Coral and Solomon Seas, located in the Southwest Pacific west of the  
694 Tonga-Kermadec Ridge remained poorly documented. This is largely due to the intricate  
695 bathymetric features and remote deep ocean basins found in the region, which make it  
696 challenging to discern the pathways of deep flow and exchanges in the region.

697 Using direct measurements of water properties from three cruises combined with WOA18  
698 historical data, this study examined the origin, the characteristics and pathways of the deep flow  
699 pattern in the Solomon Sea, and discusses their origin. Our results indicate that UCDW entering  
700 the Solomon Sea Basin through the southern entrance primarily comes from the Coral Sea Basin  
701 rather than the Central Pacific Basin, as proposed by Wyrтки (1961). At depths between 2000 and  
702 3000 m, the UCDW signature reaches as far as the New Caledonia Trough and the southernmost  
703 part of the South Fiji Basin, located west of the Tonga-Kermadec Ridge. The water property  
704 distributions indicate water mass modifications in the northern part of the Solomon Sea Basin  
705 between the southern UCDW and a flow of older and/or modified UCDW emanating from the  
706 East Caroline Basin at depths shallower than 2600 m ( $\sim 27.73 \sigma_0$ ), bringing fresher, O<sub>2</sub>-poor and  
707 SiO<sub>4</sub>-rich waters into the Solomon Sea Basin through Solomon Strait. The Solomon Sea is thus,  
708 at these depths, a region where both types of UCDW (with respectively southern and northern  
709 origins) can mix.

710 During the MoorSPICE cruise, water properties were collected at great depths in the Bismarck  
711 Sea ( $\sim 147.3^\circ\text{E}$ - $150.8^\circ\text{E}$ ,  $2.7^\circ\text{S}$ - $5.2^\circ\text{S}$ ), and clearly indicate that, below 1750 m, the Bismarck  
712 Sea is completely isolated from the large scale deep western boundary circulation in the western  
713 equatorial Pacific. Despite this lack of ventilation, the constant values of the oxygen and  
714 nutrients suggest either an absence of remineralization at depth in this closed basin, or little  
715 remineralization that is gradually compensated by downward diffusion of oxygen. In the  
716 3000-3500 m depth range, the Solomon Sea Basin is still filled by UCDW inflow directly  
717 coming from the Coral Sea Basin via a deep channel (the Pocklington Trough), and probably the  
718 UCDW that meanders from the New Hebrides and the South Fiji Basins. The deep water mass  
719 properties suggest that both UCDW inflows approach each other at the southern entrance of the  
720 Solomon Sea Basin, from where a mixture between the two UCDW appears to proceed

721 equatorward into the northern part of the basin. There, the concentrations of  $O_2$  increase with  
722 depth between 3000 to 3500 m, indicating that the densest part of UCDW imprints the high- $O_2$   
723 feature of LCDW. Below 3500 m, the water column is locally vertically homogeneous in the  
724 Solomon Sea Basin, suggesting that only UCDW supplies the near-bottom levels in the basin.  
725 This is consistent with the GEBCO 2020 bathymetric data, which indicates that LCDW is  
726 prevented by topography from spreading to the Southwest Pacific basins. In addition, the lack of  
727 oxygen consumption below 3500 m in the Solomon Sea Basin suggests that there is little or no  
728 remineralization at depth.

729 The adjusted transports estimated by inversion across the Solomon Sea are overall consistent  
730 with this circulation scheme inferred from the water properties, despite some differences in  
731 transport estimates between the Pandora and MoorSPICE cruises. We found an equatorward  
732 transport of  $5 \pm 2.6$  Sv during Pandora (in July 2012) over  $27.50$ - $27.76$   $\sigma_0$  ( $\sim 1500$ - $3250$  m),  
733 whereas weaker ( $1 \pm 1.9$  to  $2.4 \pm 1.6$  Sv) transports were found during MoorSPICE (March  
734 2014) at those densities. At Solomon Strait, the estimated transport over  $27.71$ - $27.76$   $\sigma_0$  ( $\sim$   
735  $2500$ - $3250$  m) is close to zero (within errors) during Pandora, while a southward transport of  $3 \pm$   
736  $0.8$  Sv is found during MoorSPICE. Although the Solomon Sea Basin is closed to the north  
737 below a sill depth of about 2600 m, these transport estimates provide evidence for some  
738 throughflow variability between the East Caroline and Solomon Sea Basins from 1500 m depth  
739 to the 2600 m sill-depth, which is consistent with the water mass property changes observed  
740 there. Estimates of diapycnal velocity and mixing further indicate that significant diapycnal  
741 exchanges occur throughout the Solomon Sea Basin below 2000 m depth, influencing both the  
742 water mass structure and transports of the deep flow across the basin.

743 Deeper in the water column, the abyssal flow ( $> 4000$  m) west of the Tonga-Kermadec Ridge is  
744 strongly constrained by a complex system of long and narrow deep trenches beginning southeast  
745 of New Caledonia, which then border the southern coastline of the Solomon Islands extending to  
746 the South Solomon Trench. The overall distribution of the corresponding water mass properties  
747 (i.e.,  $\theta$ , S,  $O_2$  and  $SiO_4$ ) is based only on a few historical profiles; it is, therefore, difficult to rely  
748 only on these water properties to explore the abyssal water mass structure and associated flow  
749 paths over these trenches. One may use geochemical tracers such as trace elements and isotopes  
750 to further characterize the near-bottom waters in these remote deep trenches. Nevertheless, more  
751 water property observations are required to thoroughly detail the deep and abyssal water mass  
752 distributions in the region. To this end, the recent extension of the Argo array below the typical  
753 2000 m sampling limit in the Southwest Pacific Basin (Johnson et al., 2019) offers hope for  
754 additional insights into the deep and abyssal circulation in the region.

755 **Acknowledgments**

756 The two exploratory cruises known as Pandora and MoorSPICE are contributions to the  
757 CLIVAR/SPICE and GEOTRACES International programs. The Pandora cruise has been  
758 co-funded by ANR (project ANR-09- BLAN-0233-01) and INSU/LEFE project Solwara, while  
759 the MoorSPICE cruises has been funded by the NSF grant OCE1029487. The data collected  
760 during Pandora and MoorSPICE are available online at <http://www.obs-vlfr.fr/proof/cruises.php>.  
761 MoorSPICE data can also be found online at <https://doi.org/10.7284/903044>. We thank the crews  
762 of the R/V Atalante and R/V Thomas G. Thompson. We are grateful to the engineers from the  
763 Institut de Recherche pour le Développement (IRD) US-IMAGO team, DT-INSU and Scripps  
764 Institution of Oceanography (SIO), and scientists who carefully sampled, recorded, and treated  
765 the data. Ocean historical data were freely downloaded from the World Ocean Atlas 2018  
766 (WOA18) database (<https://www.nodc.noaa.gov/OC5/woa18>). We also thank Catherine Jeandel,  
767 Valérie Chavagnac, Louis Géli and Cédric Boulart for fruitful discussions concerning the deepest  
768 water mass properties. The gridded 30 arc-second General Bathymetric Chart of the Oceans  
769 (GEBCO) 2020 bathymetry was also freely downloaded from GEBCO's website  
770 (<https://www.gebco.net>). Cyril Germineaud's work on this study was carried out in part under the  
771 auspices of the Cooperative Institute for Marine and Atmospheric Studies (CIMAS), a  
772 Cooperative Institute of the University of Miami and the National Oceanic and Atmospheric  
773 Administration (NOAA), cooperative agreement NA20OAR4320472. Cyril Germineaud also  
774 acknowledges support from the NOAA Atlantic Oceanographic and Meteorological Laboratory.

775 **References**

- 776 Albery, M. S., J. Sprintall, J. MacKinnon, A. Ganachaud, S. Cravatte, G. Eldin, C. Germineaud,  
777 and A. Melet (2017), Spatial patterns of mixing in the Solomon Sea, *Journal of Geophysical*  
778 *Research: Oceans*, 122(5), 4021-4039.
- 779 Albery, M., Sprintall, J., MacKinnon, J., Germineaud, C., Cravatte, S., & Ganachaud, A. (2019).  
780 Moored Observations of Transport in the Solomon Sea. *Journal of Geophysical Research:*  
781 *Oceans*, 124(11), 8166-8192.
- 782 Alford, M. H., J. B. Girton, G. Voet, G. S. Carter, J. B. Mickett, and J. M. Klymak (2013),  
783 Turbulent mixing and hydraulic control of abyssal water in the Samoan Passage, *Geophysical*  
784 *Research Letters*, 40(17), 4668-4674.
- 785 Callahan, J. E. (1972), The structure and circulation of deep water in the Antarctic, *Deep Sea*  
786 *Research and Oceanographic Abstracts*, 19(8), 563-575.
- 787 Cazenave, A., & Llovel, W. (2010). Contemporary sea level rise. *Annual review of marine*  
788 *science*, 2, 145-173.

789 Delpech, A., Cravatte, S., Marin, F., Morel, Y., Gronchi, E., & Kestenare, E. (2020). Observed  
790 Tracer Fields Structuration by Middepth Zonal Jets in the Tropical Pacific. *Journal of Physical*  
791 *Oceanography*, 50(2), 281-304.

792 Desbruyères, D. G., Purkey, S. G., McDonagh, E. L., Johnson, G. C., & King, B. A. (2016).  
793 Deep and abyssal ocean warming from 35 years of repeat hydrography. *Geophysical Research*  
794 *Letters*, 43(19), 10-356.

795 Ganachaud, A., & Wunsch, C. (2000). Improved estimates of global ocean circulation, heat  
796 transport and mixing from hydrographic data. *Nature*, 408(6811), 453-457.

797 Ganachaud, A. (2003), Error budget of inverse box models: The North Atlantic, *Journal of*  
798 *Atmospheric and Oceanic Technology*, 20(11), 1641-1655.

799 Ganachaud, A., Cravatte, S., Sprintall, J., Germaineaud, C., Albery, M., Jeandel, C., ... &  
800 Heimburger, L. E. (2017). The Solomon Sea: its circulation, chemistry, geochemistry and  
801 biology explored during two oceanographic cruises, *Elem. Sci. Anth.*, 5, 33.

802 Germaineaud, C., A. Ganachaud, J. Sprintall, S. Cravatte, G. Eldin, M. S. Albery, and E. Privat  
803 (2016), Pathways and water mass properties of the thermocline and intermediate waters in the  
804 Solomon Sea, *Journal of Physical Oceanography*, 46(10), 3031-3049.

805 Halunen Jr, A. J., & Von Herzen, R. P. (1973). Heat flow in the western equatorial Pacific Ocean.  
806 *Journal of Geophysical Research*, 78(23), 5195-5208.

807 Hood, E., C. Sabine, and B. Sloyan (2010), The go-ship repeat hydrography manual: A  
808 collection of expert reports and guidelines, IOCCP Rep, 14.

809 Johnson, G. C. (2008), Quantifying Antarctic Bottom Water and North Atlantic deep water  
810 volumes, *Journal of Geophysical Research: Oceans*, 113(C5), c05027.

811 Johnson, G. C., and J. M. Toole (1993), Flow of deep and bottom waters in the Pacific at 10°N,  
812 *Deep Sea Research Part I: Oceanographic Research Papers*, 40, 371-394.

813 Johnson, H. P., Hautala, S. L., Bjorklund, T. A., & Zarnetske, M. R. (2006). Quantifying the  
814 North Pacific silica plume. *Geochemistry, Geophysics, Geosystems*, 7(5).



815 Johnson, G. C., J. M. Lyman, and S. G. Purkey (2015), Informing deep argo array design using  
816 argo and full-depth hydrographic section data, *Journal of Atmospheric and Oceanic Technology*,  
817 32(11), 2187-2198.

818 Johnson, G. C., Purkey, S. G., Zilberman, N. V., & Roemmich, D. (2019). Deep Argo quantifies  
819 bottom water warming rates in the Southwest Pacific Basin. *Geophysical Research Letters*,  
820 46(5), 2662-2669.

821 Joshima, M., & Honza, E. (1986). Age estimation of the Solomon Sea based on heat flow data.  
822 *Geo-marine letters*, 6(4), 211-217.

823 Kawabe, M., and S. Fujio (2010), Pacific Ocean circulation based on observation, *Journal of*  
824 *Oceanography*, 66(3), 389-403.

825 Kawabe, M., D. Yanagimoto, and S. Kitagawa (2006), Variations of deep western boundary  
826 currents in the melanesian basin in the western North Pacific, *Deep Sea Research Part I:*  
827 *Oceanographic Research Papers*, 53(6), 942-959.

828 Kawabe, M., S. Fujio, D. Yanagimoto, and K. Tanaka (2009), Water masses and currents of deep  
829 circulation southwest of the Shatsky Rise in the western North Pacific, *Deep Sea Research Part*  
830 *I: Oceanographic Research Papers*, 56(10), 1675-1687.

831 Kunze, E., Firing, E., Hummon, J. M., Chereskin, T. K., & Thurnherr, A. M. (2006). Global  
832 abyssal mixing inferred from lowered ADCP shear and CTD strain profiles. *Journal of Physical*  
833 *Oceanography*, 36(8), 1553-1576.

834 Langdon, C. (2010), Determination of dissolved oxygen in Seawater by Winkler Titration  
835 using the Amperometric Technique, The GO-SHIP Repeat Hydrography Manual: A Collection  
836 of Expert Reports and Guidelines IOCCP Report no 14, GO-SHIP.ORG, version1.

837 Lindstrom, E., R. Lukas, R. A. Fine, J. S. Godfrey, G. Meyers, and M. Tsuchiya, 1987: The  
838 Western Equatorial Pacific Ocean Circulation Study. *Nature*, 330, 533–537.

839 Lumpkin, R., & Speer, K. (2007). Global ocean meridional overturning. *Journal of Physical*  
840 *Oceanography*, 37(10), 2550-2562.

841 Mantyla, A. W., and J. L. Reid (1983), Abyssal characteristics of the world ocean waters, *Deep*  
842 *Sea Research Part A. Oceanographic Research Papers*, 30(8), 805-833.

843 Meinen, C. S., Perez, R. C., Dong, S., Piola, A. R., & Campos, E. (2020). Observed ocean  
844 bottom temperature variability at four sites in the northwestern Argentine Basin: Evidence of  
845 decadal deep/abyssal warming amidst hourly to interannual variability during 2009-2019.  
846 *Geophysical Research Letters*, e2020GL089093.

847 Melet, A., J. Verron, L. Gourdeau, and A. Koch-Larrouy (2011), Equatorward pathways of  
848 Solomon Sea water masses and their modifications, *Journal of Physical Oceanography*, 41,  
849 810-826.

850 Orsi, A. H., G. C. Johnson, and J. L. Bullister (1999), Circulation, mixing, and production of  
851 Antarctic Bottom Water, *Progress in Oceanography*, 43(1), 55-109.

852 Peltier, W. R., & Caulfield, C. P. (2003). Mixing efficiency in stratified shear flows. *Annual*  
853 *review of fluid mechanics*, 35(1), 135-167.

854 Polzin, K. L., Garabato, A. C. N., Huussen, T. N., Sloyan, B. M., & Waterman, S. (2014).  
855 Finescale parameterizations of turbulent dissipation. *Journal of Geophysical Research: Oceans*,  
856 119(2), 1383-1419.

857 Purkey, S. G., & Johnson, G. C. (2010). Warming of global abyssal and deep Southern Ocean  
858 waters between the 1990s and 2000s: Contributions to global heat and sea level rise budgets.  
859 *Journal of Climate*, 23(23), 6336-6351.

860 Purkey, S. G., Johnson, G. C., Talley, L. D., Sloyan, B. M., Wijffels, S. E., Smethie, W., et al.  
861 (2019). Unabated Bottom Water Warming and Freshening in the South Pacific Ocean. *Journal of*  
862 *Geophysical Research: Oceans*, 124, 1778-1794.

863 Reid, J. L. (1986), On the total geostrophic circulation of the south Pacific Ocean: Flow patterns,  
864 tracers and transports, *Progress in Oceanography*, 16(1), 1-61.

865 Reid, J. L. (1997), On the total geostrophic circulation of the Pacific Ocean: flow patterns,  
866 tracers, and transports, *Progress in Oceanography*, 39(4), 263-352.

867 Ridgway, K., J. Dunn, and J. Wilkin (2002), Ocean interpolation by four-dimensional weighted  
868 least squares-application to the waters around Australia, *Journal of atmospheric and oceanic*  
869 *technology*, 19(9), 1357-1375.

870 Roemmich, D., S. Hautala, and D. Rudnick (1996), Northward abyssal transport through the  
871 Samoan Passage and adjacent regions, *Journal of Geophysical Research: Oceans*, 101(C6),  
872 14,039-14,055.

873 Rudnick, D. L. (1997), Direct velocity measurements in the Samoan Passage, *Journal of*  
874 *Geophysical Research: Oceans*, 102(C2), 3293-3302.

875 Saout-Grit, C., A. Ganachaud, C. Maes, L. Finot, L. Jamet, F. Baurand, and J. Grelet (2015),  
876 Calibration of CTD oxygen data collected in the Coral Sea during the 2012 bifurcation cruise,  
877 Mercator Ocean-Coriolis Quarterly Newsletter Special Issue, 52(3), 27-33.

878 Siedler, G., J. Holfort, W. Zenk, T. J. Müller, and T. Csernok (2004), Deep-Water flow in the  
879 Mariana and Caroline Basins, *Journal of Physical Oceanography*, 34(3), 566-581.

880 Sokolov, S., and S. Rintoul (2000), Circulation and water masses of the southwest Pacific:  
881 WOCE section P11, Papua New Guinea to Tasmania, *Journal of marine research*, 58(2),  
882 223-268.

883 Taft, B. A., S. P. Hayes, G. E. Friederich, and L. A. Codispoti (1991), Flow of abyssal water into  
884 the Samoa Passage, *Deep Sea Research Part A. Oceanographic Research Papers*, 38,  
885 S103-S128.

886 Talley, L. D., and T. M. Joyce (1992), The double silica maximum in the North Pacific, *Journal*  
887 *of Geophysical Research: Oceans*, 97(C4), 5465-5480.

888 Talley, L. D., M. D. Sparrow, P. Chapman, and J. Gould (2007), Hydrographic atlas of the World  
889 Ocean Circulation Experiment (WOCE): Volume 2: Pacific Ocean, WOCE International Project  
890 Office.

891 Toole, J. M., R. W. Schmitt, and K. L. Polzin (1994), Estimates of diapycnal mixing in the  
892 abyssal ocean, *Science*, 264(5162), 1120.

893 Tsimplis, M. N., S. Bacon, and H. L. Bryden (1998), The circulation of the subtropical South  
894 Pacific derived from hydrographic data, *Journal of Geophysical Research: Oceans*, 103(C10),  
895 21,443-21,468.

896 Tsuchiya, M. (1991). Flow path of the Antarctic Intermediate Water in the western equatorial  
897 South Pacific Ocean. *Deep Sea Research Part A. Oceanographic Research Papers*, 38,  
898 S273-S279.

899 Uchida, H., C. G. Johnson, and K. E. McTaggart (2010), CTD oxygen sensor calibration  
900 procedures, The GO-SHIP Repeat Hydrography Manual: A Collection of Expert Reports and  
901 Guidelines IOCCP Report no 14, GO-SHIP.ORG, version 1.

902 Visbeck, M. (2002), Deep velocity profiling using Acoustic Doppler Current Profilers: Bottom  
903 tracks and inverse solutions., *Journal of Atmospheric and Oceanic Technology*, 19, 794-807.

904 Voet, G., J. B. Girton, M. H. Alford, G. S. Carter, J. M. Klymak, and J. B. Mickett (2014),  
905 Pathways, volume transport, and mixing of abyssal water in the Samoan Passage, *Journal of*  
906 *Physical Oceanography*, 45(2), 562-588.

907 Voet, G., M. H. Alford, J. B. Girton, G. S. Carter, J. B. Mickett, and J. M. Klymak (2016),  
908 Warming and weakening of the abyssal flow through Samoan Passage, *Journal of Physical*  
909 *Oceanography*, 46(8), 2389-2401.

910 Warren, B. A. (1973), Transpacific hydrographic sections at Lats. 43°S and 28°S: the SCORPIO  
911 expedition II. deep water, *Deep Sea Research and Oceanographic Abstracts*, 20(1), 9-38.

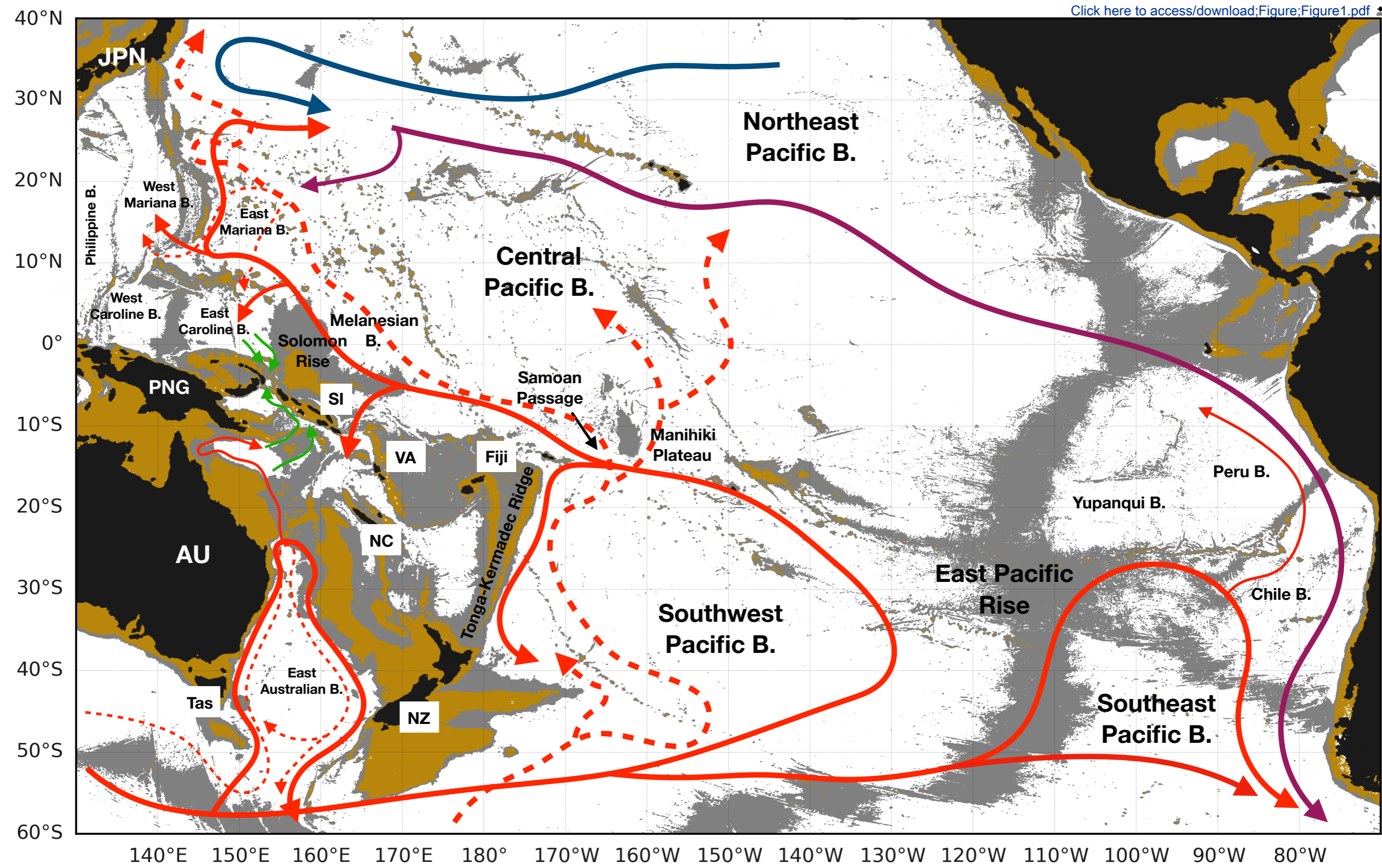
912 Whitworth III, T., B. A. Warren, W. D. Nowlin, Jr, S. B. Rutz, R. D. Pillsbury, and M. I. Moore  
913 (1999), On the deep western-boundary current in the southwest Pacific Basin, *Progress in*  
914 *Oceanography*, 43(1), 1-54.

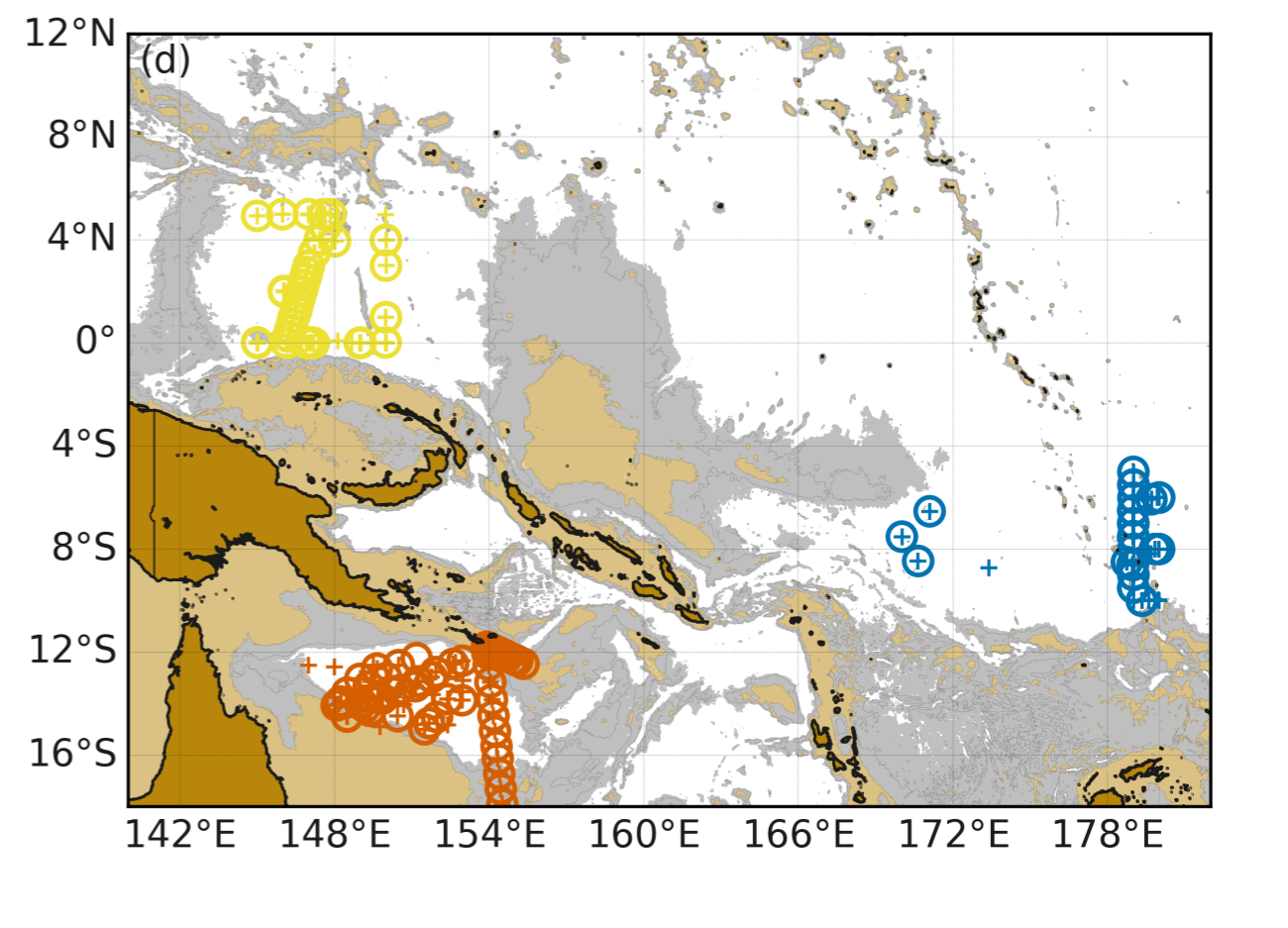
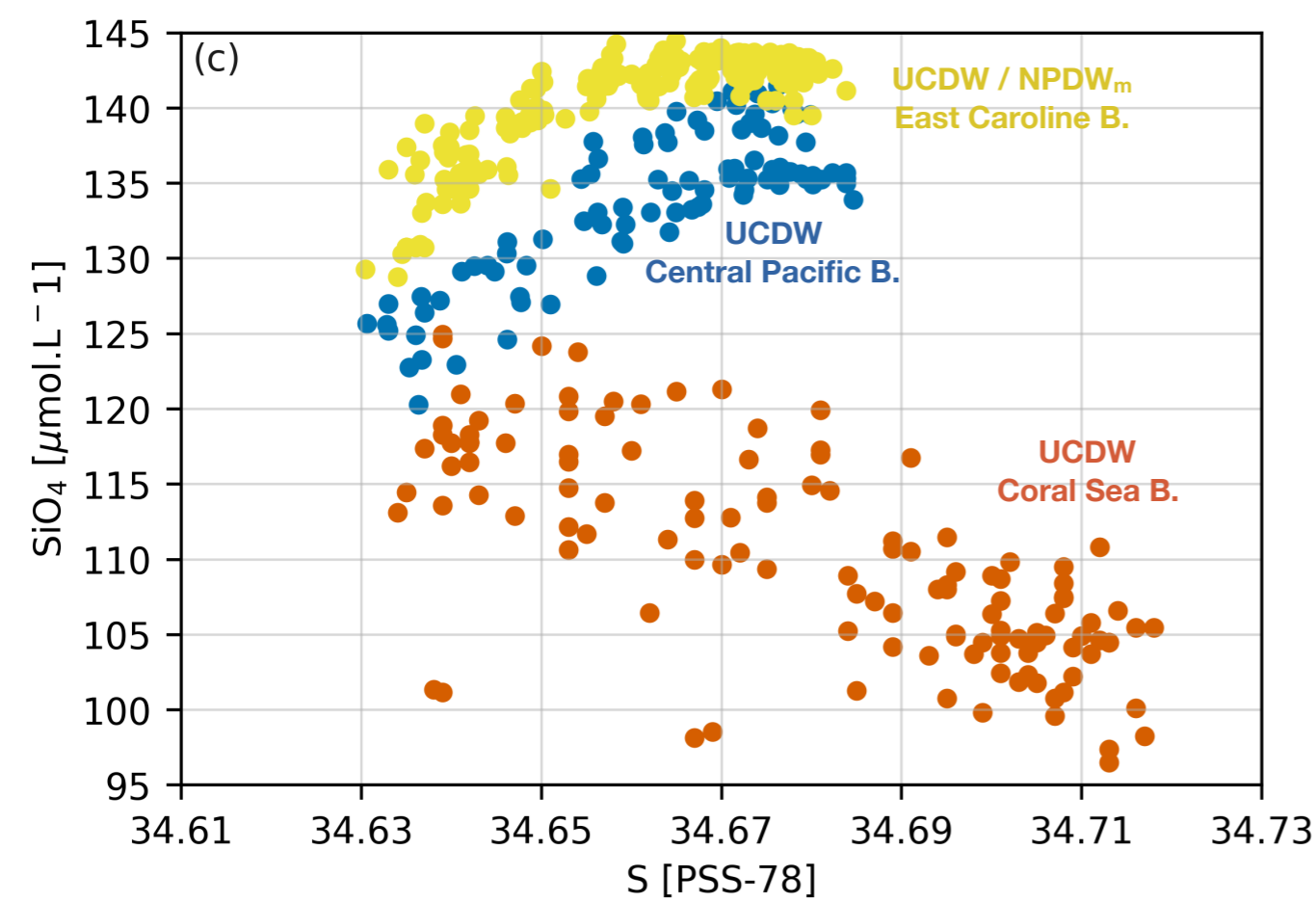
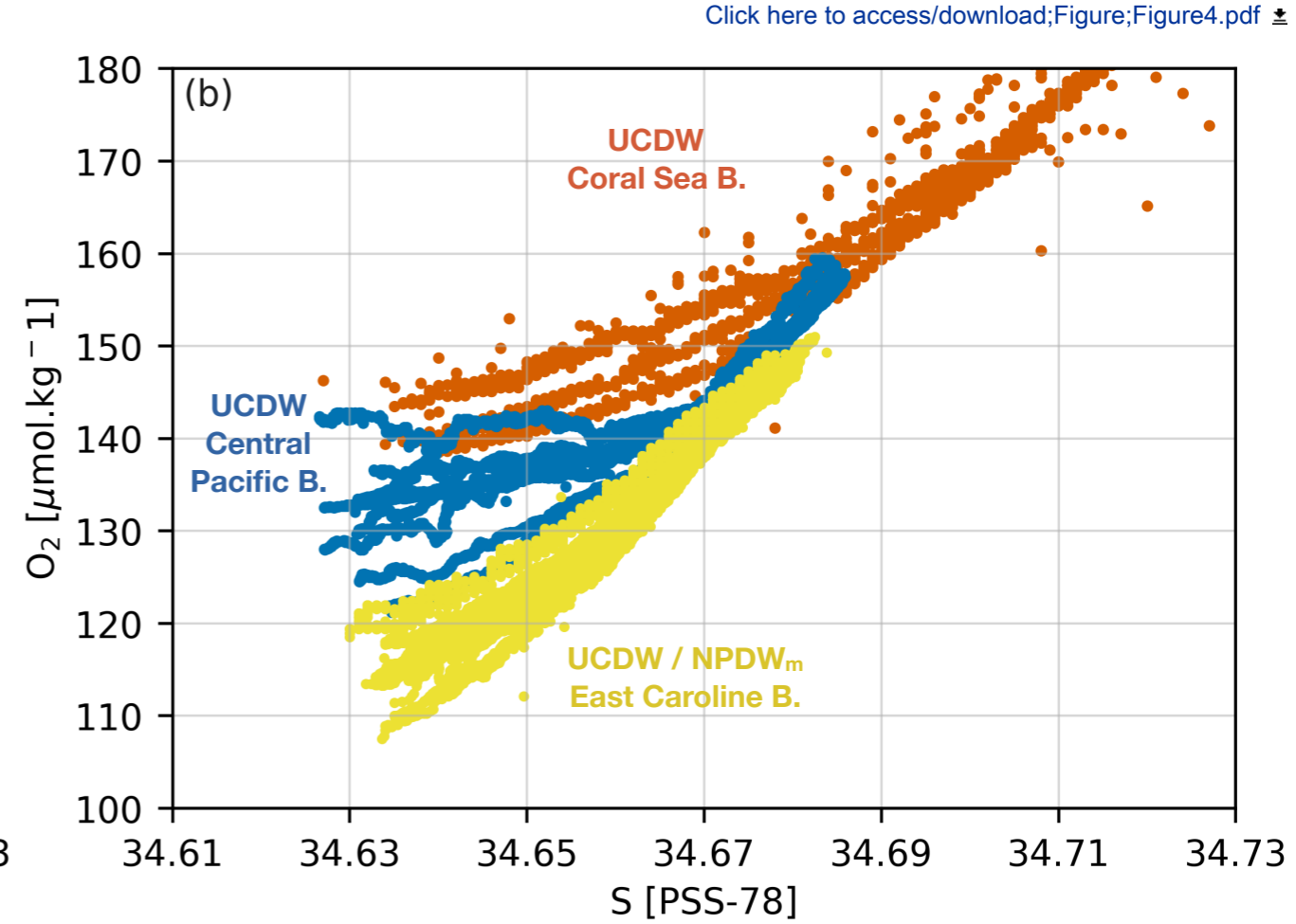
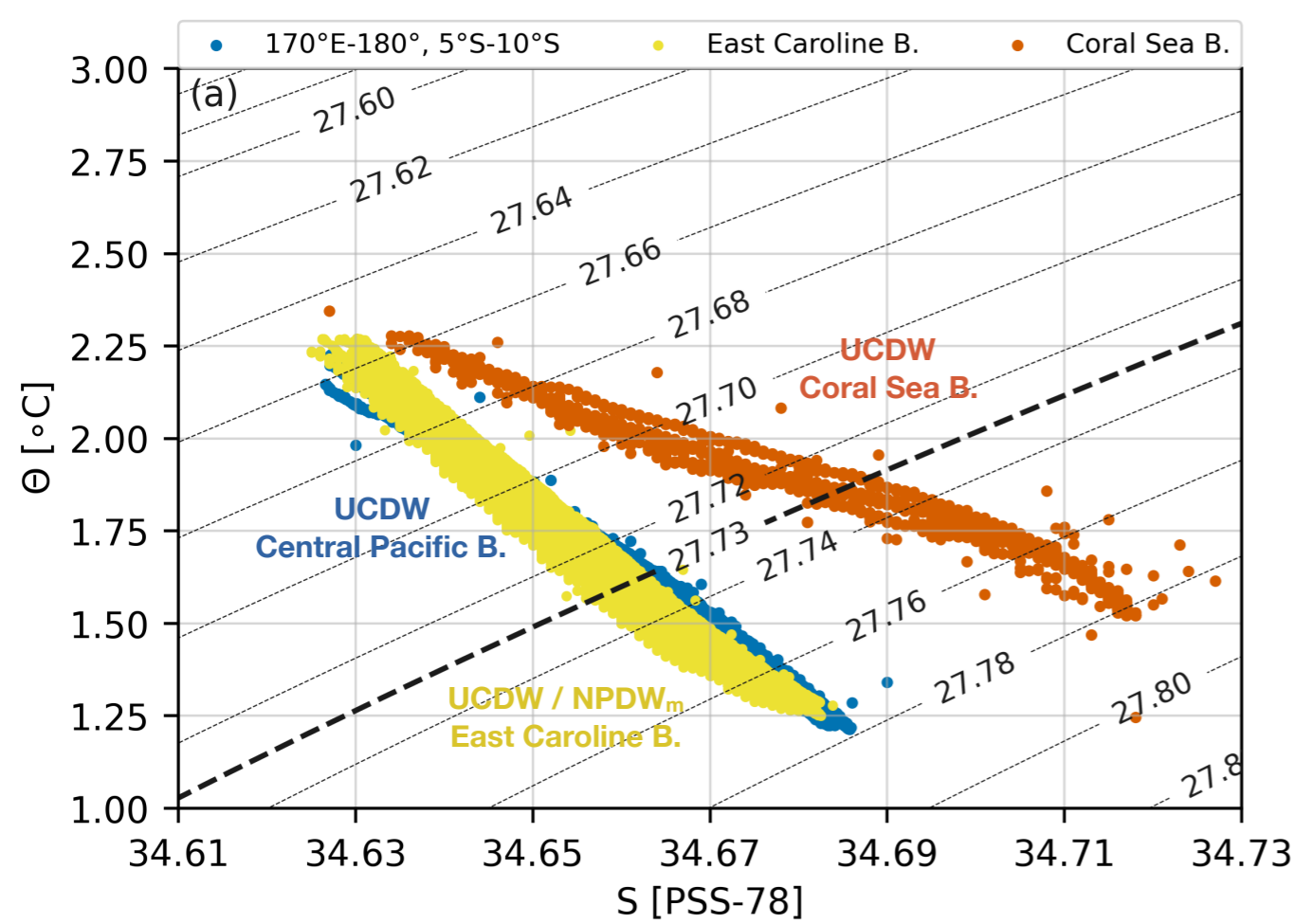
915 Wijffels, S. E., M. M. Hall, T. Joyce, D. J. Torres, P. Hacker, and E. Firing (1998), Multiple deep  
916 gyres of the western North Pacific: A woce section along 149°E, *Journal of Geophysical*  
917 *Research: Oceans*, 103(C6), 12, 985-13,009.

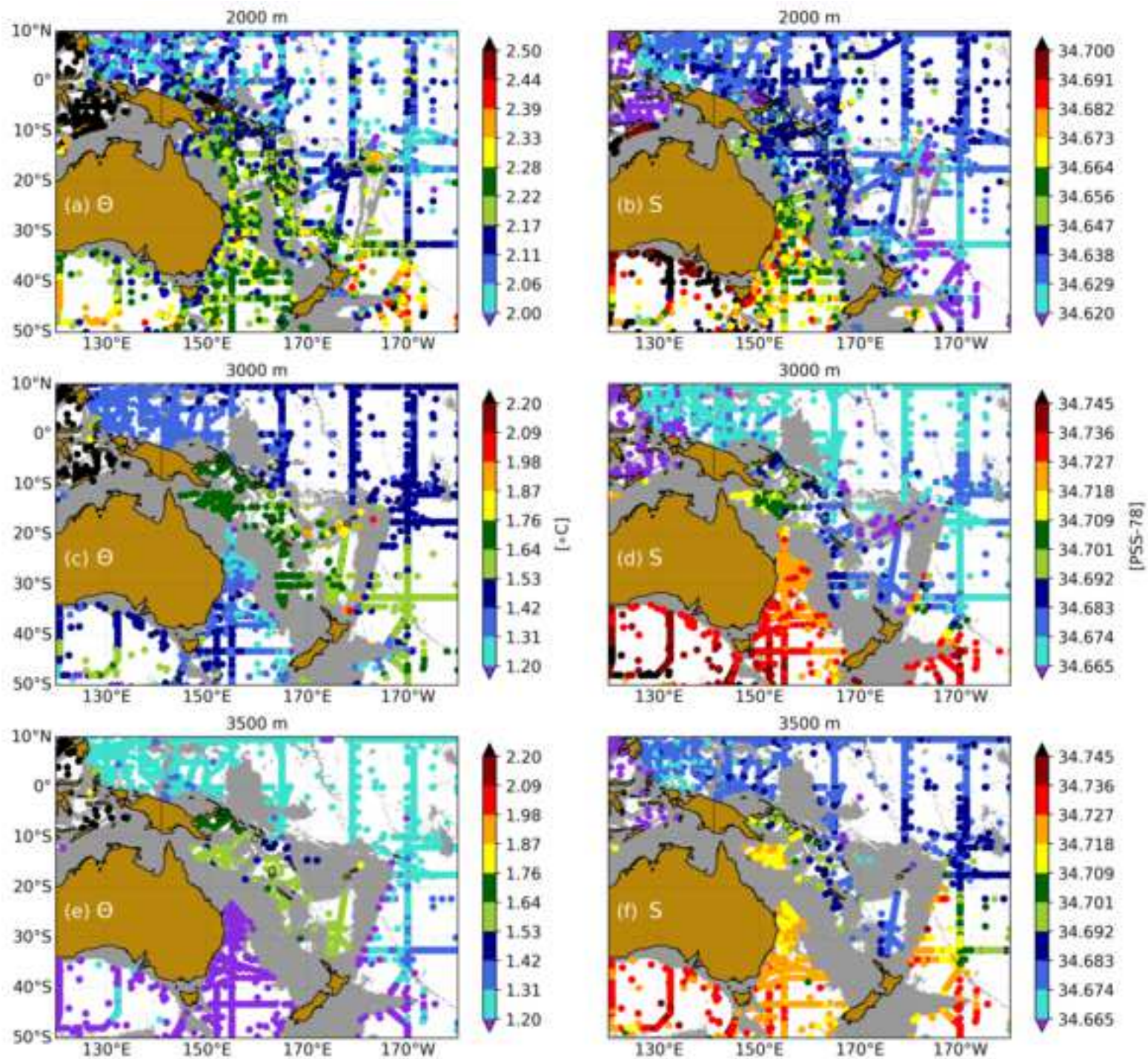
918 Wijffels, S. E., J. M. Toole, and R. Davis (2001), Revisiting the south pacific subtropical  
919 circulation: A synthesis of world ocean circulation experiment observations along 32°S, *Journal*  
920 *of Geophysical Research: Oceans*, 106(C9), 19, 481-19,513.

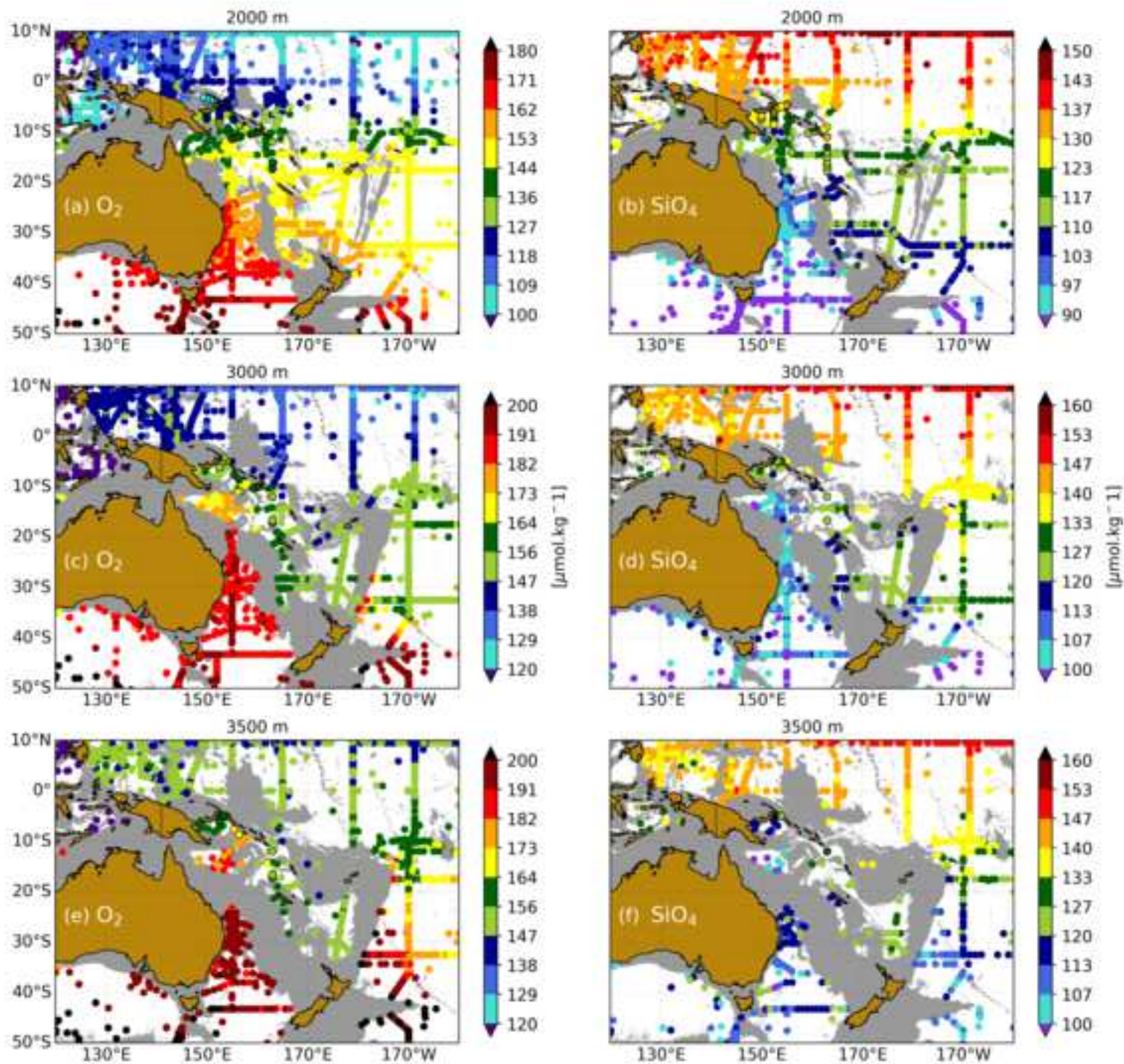
921 Wunsch, C. (1996). *The ocean circulation inverse problem*. Cambridge University Press, 442 pp.

922 Wyrtki, K. (1961). The flow of water into the deep sea basins of the western South Pacific  
923 Ocean. *Marine and Freshwater Research*, 12(1), 1-16.

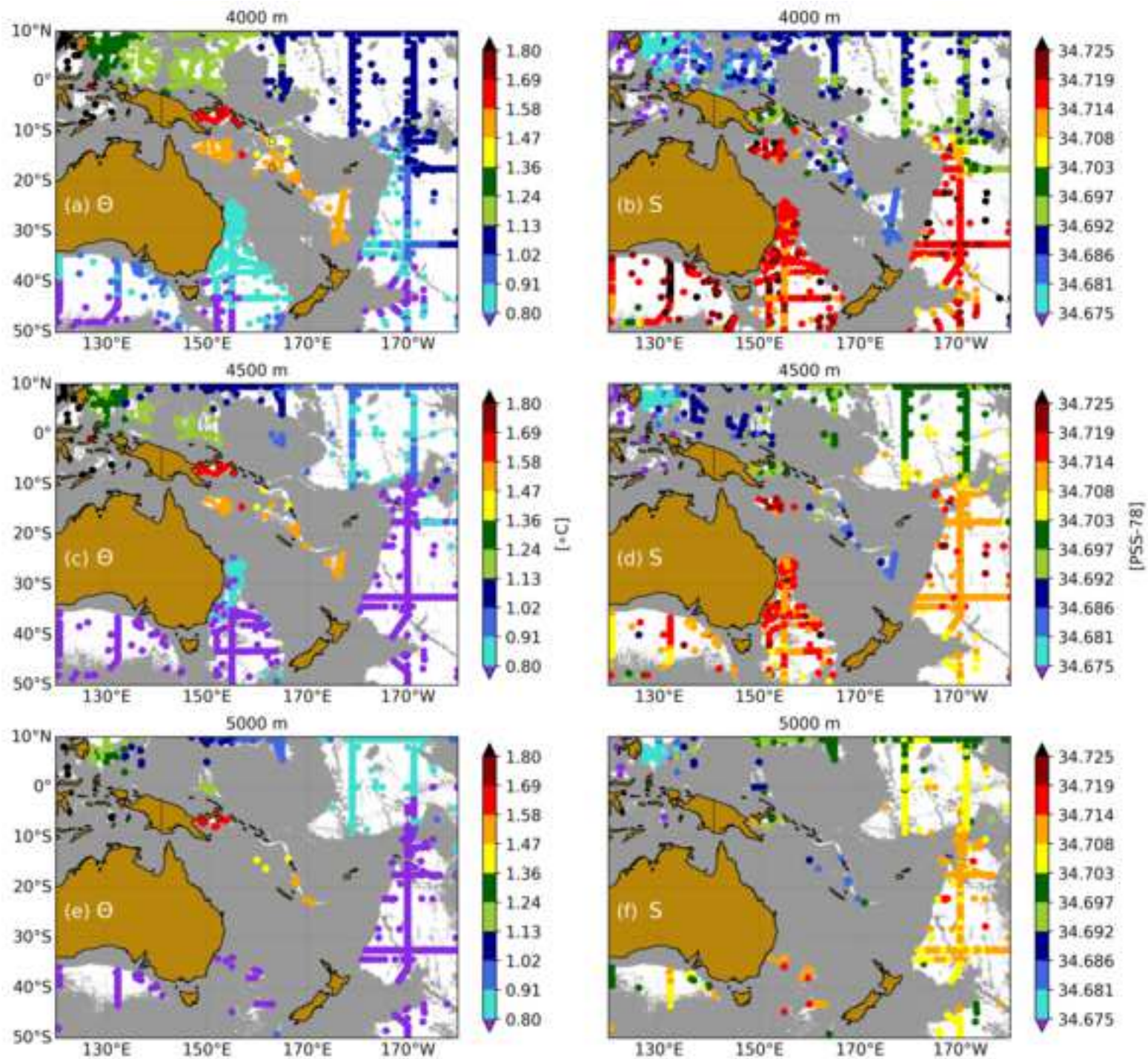


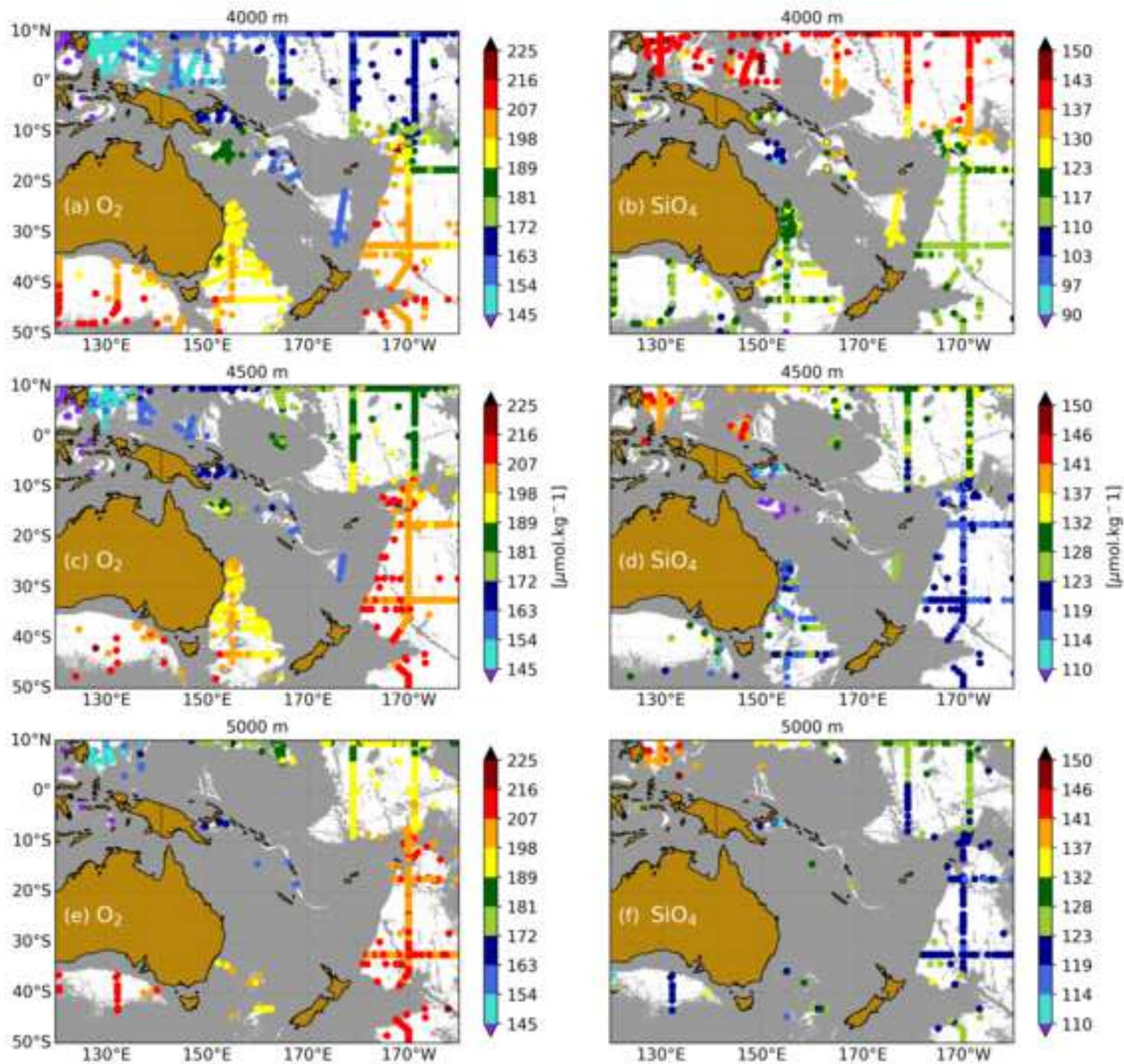


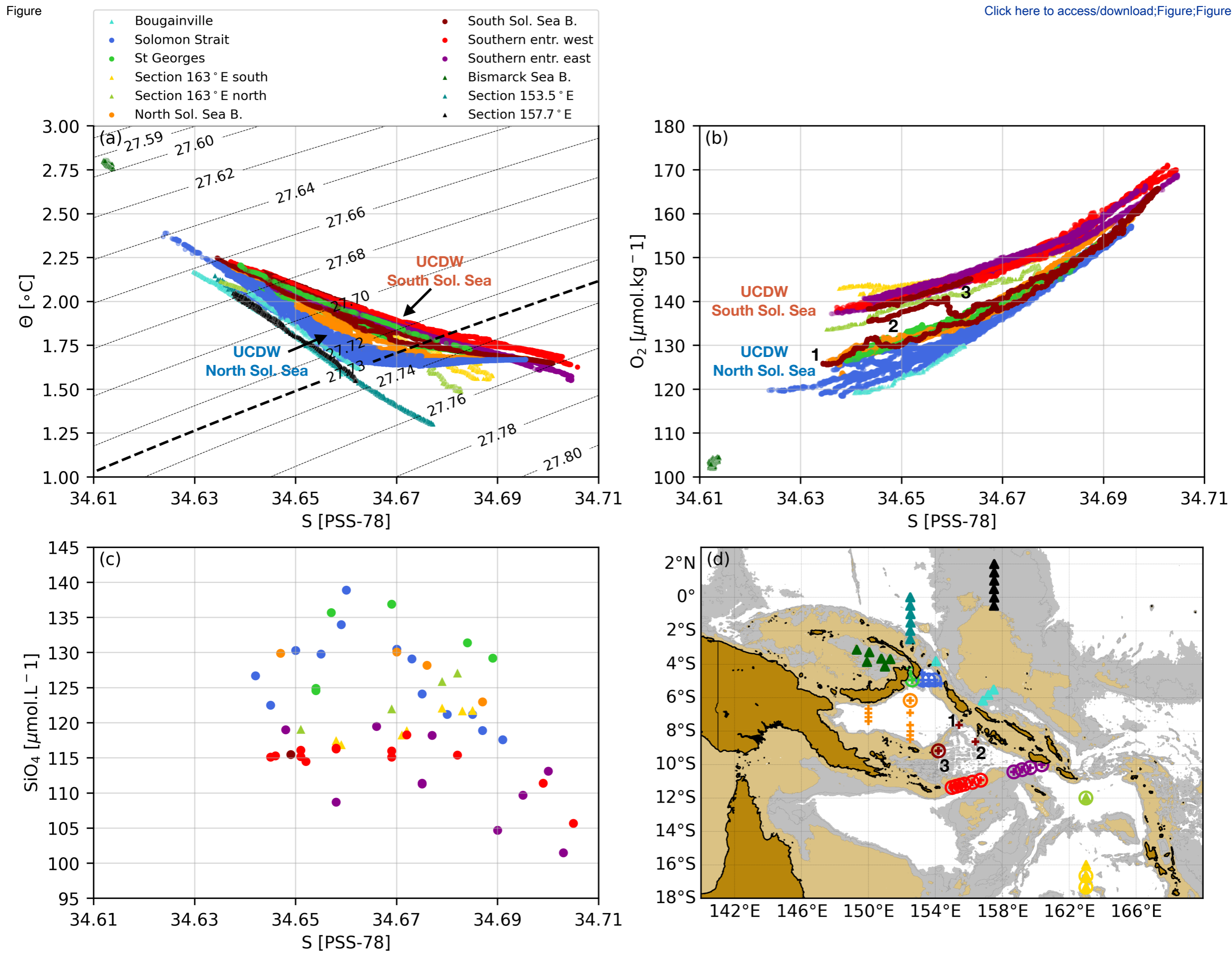














Click here to access/download


**Supplementary Material**

SI\_Deep\_pacific\_circulation\_solomon\_sea\_R1.pdf





Click here to access/download  
**Supplementary Material**  
FigureS1.png



Click here to access/download  
**Supplementary Material**  
FigureS2.png



Click here to access/download  
**Supplementary Material**  
FigureS3.png



Click here to access/download  
**Supplementary Material**  
FigureS4.png





Click here to access/download  
**Supplementary Material**  
FigureS5.png



Click here to access/download  
**Supplementary Material**  
FigureS6.png

**Declaration of interests**

The authors declare that they have no known competing financial interests or personal relationships that could have appeared to influence the work reported in this paper.

The authors declare the following financial interests/personal relationships which may be considered as potential competing interests: